RNA Editors Sculpt the Transcriptome During Terminal Erythropoiesis

Areum Han[1,2], Alena Yermalovich[3,4], Mohamad Ali T. Najia[1,4,5,6], Daniel S. Pearson[7], Yuko Fujiwara[10,11], Michael Bolgov[1], Caroline Kubaczka[6], Trista E. North[6,8], Vanessa Lundin[9], Stuart Orkin[10, 11], George Q. Daley[1,2,6*]

[1]Division of Hematology/Oncology, Boston Children's Hospital, Boston, MA, USA. [2]Department of Biological Chemistry and Molecular Pharmacology, Harvard Medical School, Boston, MA, USA. [3]Department of Medical Oncology, Dana-Farber Cancer Institute, Boston, MA, USA. [4]Broad Institute of Harvard and MIT, Cambridge, MA, USA. [5] Harvard-MIT Division of Health Sciences and Technology, Massachusetts Institute of Technology, Cambridge, MA, USA. [6]Stem Cell Program, Boston Children's Hospital, Boston, MA, USA. [7]Department of Pathology, Massachusetts General Hospital, Boston, MA, USA. [8]Developmental and Regenerative Biology Program, Harvard Medical School, Boston, MA, USA. [9]Center for Hematology and Regenerative Medicine, Department of Medicine Huddinge, Karolinska Institutet, Huddinge, Sweden. [10]Dana-Farber/Boston Children's Hospital Cancer and Blood Disorder Center, Department of Pediatrics, Harvard Medical School, Boston, MA, USA. [11]Howard Hughes Medical Institute, Harvard Medical School, Boston, MA, USA.

*Corresponding author: george.daley@childrens.harvard.edu

ABSTRACT

Selective RNA degradation during terminal erythropoiesis results in a globin-rich transcriptome in mature erythrocytes, but the specific RNA decay pathways remain unknown. We found that deficiency of the terminal uridylyl transferase enzyme Zcchc6 and the 3'-5' exoribonuclease Dis3l2 in mouse models led to fetal and perinatal reticulocytosis, an accumulation of RNA-rich precursors of terminal erythroid cells, suggesting their crucial roles in terminal red cell differentiation. Notably, knockout embryos exhibited persistent high-level expression of *Hbb-bh1* globin, the ortholog of human fetal *γ*-globin. Perturbation of the Zcchc6-Dis3l2 pathway in mice engineered to express the human β-globin locus likewise increased *γ*-globin levels in fetal erythroid cells, suggesting that globin switching entails post-transcriptional mechanisms of mRNA destabilization in addition to transcriptional down-regulation. We cultured human hematopoietic stem and progenitor cells (HSPCs), performed CRISPR/Cas9-mediated knockout of ZCCHC6 and DIS3L2, and observed accumulation of RNA and elevated γ-globin levels in terminal erythroid cells. Our findings reveal a conserved role for the

ZCCHC6/DIS3L2 RNA editors in terminal erythropoiesis and demonstrate a post-transcriptional mechanism for *γ*-globin gene switching, advancing research into *in vitro* erythrocyte generation and *γ*-globin stabilization to ameliorate hemoglobinopathies.

INTRODUCTION

Terminal differentiation of red blood cells (RBCs)[1,2] entails the loss of key cellular components such as the nucleus, mitochondria, and ribosomes[3–7]. After enucleation, orthochromatic erythroid cells become reticulocytes, which then undergo extensive RNA degradation to develop into mature erythrocytes, primarily composed of globins[8]. Previous examination of RNA half-life suggests that active decay of non-erythrocyte transcripts contributes to this globin-rich, low-entropy transcriptome[9,10], in addition to global proteome remodeling through protein tagging by ubiquitination[11].

The Terminal Uridylyl Transferase ZCCHC6 (TUTase 7) has recently been implicated in regulating the degradation of various RNAs during cellular transitions, rather than in steady-state conditions[12–20]. This re-sculpting of the transcriptome occurs in transcriptionally compromised or quiescent contexts, such as when cells are treated with the transcription inhibitor Actinomycin D[21] or during the maternal-to-zygotic transition (MZT)[22]. During MZT, a sharp decline in maternal transcripts accelerates the emergence of the zygotic transcriptome. This coordinated transcriptome remodeling is comparable to the terminal stages of erythropoiesis.

Embryonic, fetal, and adult hemoglobins are sequentially expressed during mouse and human erythroid ontogeny[23]. In humans, during the switch from fetal globin (HbF; α2γ2) to adult globin (α2β2), γ-globins are replaced by adult β-globins. Conversely, faulty adult β-globin with pathogenic mutations can be rescued by reactivating γ-globin expression. Indeed, elevated γ-globin levels in adults have been shown to ameliorate symptoms of sickle cell disease[24,25]. Due to this therapeutic potential, the transcriptional regulation of γ-globin has been extensively studied[26,27], while its post-transcriptional regulation remains less explored[28,29].

Prior studies have shown that the ZCCHC6 adds uridines to the 3' end of target RNAs, which serves as a recognition signal for the 3′ to 5′ exonuclease DIS3L2, leading to the degradation of target RNAs[12,18,30,31]. *Zcchc6*, uniquely recognized for its

68 RNA-tagging capability, is upregulated in the peripheral blood of mice exposed to chronic
69 hypoxia and subsequently downregulated during normoxic recovery [32], suggesting that
70 increased levels of ZCCHC6 might be necessary to process the higher number of
71 reticulocytes generated during erythropoietic stress. ZCCHC6 appears to be a rate-
72 limiting factor in RNA editing, as it is slower than nuclease activity. Based on all the above,
73 we posited that the ZCCHC6-DIS3L2 axis might regulate RNA fate during terminal
74 erythropoiesis, accelerating RNA degradation and potentially influencing globin switching.
75 In this study, we explored the role of the RNA editor-exonuclease axis during terminal
76 erythropoiesis using murine models and in vitro erythroid differentiation of human blood
77 progenitors. Our findings revealed that loss of this axis leads to RNA accumulation and
78 upregulation of fetal globin expression, resulting in a reversed globin switching pattern
79 during terminal erythropoiesis. This highlights a novel, conserved post-transcriptional
80 gene regulation pathway during late erythropoiesis.
81

82 ## RESULTS

83 ### Whole-body *Zcchc6/Dis3l2* KO mice exhibit reticulocytosis and anemia.

84 We began our investigation by analyzing the expression profiles of Zcchc6 and
85 Dis3L2 throughout erythropoietic ontogeny, examining blood from knockout (KO)
86 models across embryonic stages to adulthood. Analysis of a public dataset
87 demonstrated that the expression of *Zcchc6* is upregulated as erythroid cells
88 differentiate into the terminal stages of fetal and adult definitive erythropoiesis[33,34]
89 (Extended Data Fig. 1, upper panel), suggesting that Zcchc6 plays an important role in
90 terminal erythropoiesis. In contrast, *Dis3l2* did not show high expression in the terminal
91 stages (Extended Data Fig. 1, lower panel). As an exonuclease, Dis3L2 may not be a
92 limiting factor in RNA regulation.
93 We generated a whole-body *Dis3l2* KO model (Extended Data Fig. 2), but the
94 *Dis3l2* KOs exhibited postnatal lethality. Adult *Zcchc6* KOs survived and demonstrated
95 an increase in reticulocytes compared to wild-type (WT) controls, suggesting a role for
96 Zcchc6 during the transition from reticulocytes to mature RBCs (Extended Data Fig. 3c).
97 Other hematological parameters in the *Zcchc6* KO were mostly comparable to those of
98 the WT in young adult stages (Extended Data Fig. 3 a&b). Zcchc6 KO animals exhibited

99 increased neutrophil counts compared to heterozygous (HET) animals (Extended Data
100 Fig. 3b).
101 At embryonic day (E) 18.5, cells are undergoing RNA degradation as they
102 differentiate from reticulocytes to erythrocytes, and both KOs are viable. Therefore, we
103 investigated animals at this age and observed embryonic anemia and reticulocytosis in
104 both KO models. In detail, we collected peripheral blood and spleen cells from E18.5
105 embryos, and performed histology, flow cytometry, and hemogram analysis (Fig.1a).
106 Examination of blood smears from *Zcchc6* and *Dis3l2* KO embryos showed
107 polychromasia and increased RNA retention in red cells, as revealed by staining with
108 methylene blue, indicating reticulocytosis (Fig.1b). We quantified reticulocytosis using
109 flow cytometry, pre-gating erythroid (TER119+) cells and staining for the CD71
110 transferrin receptor and the nucleic acid dye Thiazole Orange (TO) [35,36] (Fig.1c). WTs
111 displayed expected patterns of CD71 loss and RNA (TO signal) loss, while KOs showed
112 higher levels of RNA and a significantly higher $CD71^{low}TO^{high}$ population relative to
113 HETs and WTs (Fig.1c). These data demonstrate that Zcchc6 and Dis3l2 impact RNA
114 degradation during terminal erythropoiesis. We also profiled erythroid RNA dynamics in
115 the embryonic spleen, an erythropoietic organ at E18.5[37]. Embryonic spleen
116 harbors nucleated erythroid cells, and we observed a large drop in TO signal in the
117 $CD71^{high}$ population due to enucleation[35] (Extended Data Fig.4a). However, we did not
118 observe differences in enucleation ratio across genotypes. On the other hand, in the
119 later stage of erythroid cell differentiation ($TER119^{+}CD71^{low}$), the $CD71^{low}TO^{high}$
120 population was elevated in KOs compared to HETs and WTs (Extended Data Fig.4a),
121 again indicating inefficient RNA degradation in KOs. In both peripheral blood and
122 spleen, this accumulation of the $CD71^{low}TO^{high}$ population was genotype-dependent on
123 Zcchc6 (Extended Data Fig.4a, right graph). This result suggests that cellular levels of
124 Zcchc6 determine the extent of RNA degradation.
125 Both KOs at E18.5 had reduced RBC numbers, decreased hematocrit (HCT) and
126 increased Mean Corpuscular Hemoglobin (MCH) compared to HETs and WTs (Fig.1d).
127 *Zcchc6* KO also showed increased Red Cell Distribution Width (RDW); a trend observed
128 in *Dis3l2* KO that failed to reach statistical significance in WT. For *Dis3l2* KOs, we
129 observed a significant increase in Mean Corpuscular Volume (MCV) and lower

130 hemoglobin concentration (Hb), a trend also observed in *Zcchc6* KOs but without
131 statistical significance. Both KOs were anemic from a reduced number of RBCs, and both
132 showed lymphocytosis (Extended Data Fig. 4b). *Zcchc6* KO generally showed more
133 marked differences in the leukocyte panel with an increased absolute number and
134 percentage of monocytes (MO), a decreased percentage of basophils (BA), and
135 increased number in neutrophils (NE). These interesting observations could be further
136 examined in future studies.
137

138 **Conditional *Zcchc6/Dis3l2* KO mice phenocopy whole-body KOs.**

139 To examine erythrocyte-specific phenotypes, we utilized animals in which the
140 *Zcchc6/Dis3l2* alleles were flanked by LoxP sites (floxed) to generate conditional
141 KOs of these genes by crossing to strains expressing *EpoR-Cre* [38] (Fig. 2a & Extended
142 Data Fig. 2). Conditional KO in erythroid cells (TER119+) was confirmed by western blot
143 (Extended Data Fig. 2b). Indeed, cKOs phenocopied the reticulocytosis observed in
144 whole-body KOs (Fig. 2b), indicating that this phenotype is cell-autonomous. Both cKOs
145 exhibited a statistically significant increase in the $CD71^{low}TO^{high}$ population in peripheral
146 blood (Fig. 2b) and spleen (Extended Data Fig. 5a) compared to *EpoR-Cre*-carrying and
147 cWT animals. Hematological readings in both cKOs showed consistent reduction in
148 RBC numbers (Fig. 2c). cKOs again showed a trend of increased absolute WBC
149 numbers, specifically in the absolute number of lymphocytes (Extended Data Fig. 5b).
150 To demonstrate that the observed reticulocytosis reflected failed red cell maturation and
151 not hemolytic anemia, we confirmed preserved levels of haptoglobin and the absence of
152 elevated LDH and bilirubin levels [39] (Extended Data Fig. 6). Taken together, these
153 results indicate that the observed reticulocytosis arises from an RNA degradation defect
154 intrinsic to the erythroid cell during terminal differentiation.
155

156 **Normal terminal erythropoiesis in KO mice lacking *Lin28a/b* and *Zcchc11*.**

157 An enzymatic axis regulating microRNA biogenesis has been described whereby
158 the RNA binding proteins LIN28A/B dock to the loop of the microRNA precursor *pre-let-*
159 *7*, which then recruits ZCCHC6 or the paralog ZCCHC11, resulting in an inhibitory tri-
160 complex[18]. The assembled tri-complex facilitates oligouridylation, and the

161 oligouridylated RNA species then become substrates for DIS3L2[30] (Extended Data Fig.
162 7a). However, neither *Lin28a* nor *Lin28b* KOs exhibited reticulocytosis (Extended Data
163 Fig. 7b). Paralogs often perform similar functions and manifest redundancy. Among
164 seven TUTases in humans, ZCCHC6 and ZCCHC11 are the two largest TUTases with
165 CCHC and C2H2-type zinc finger domains[18]. Previous studies have shown that
166 ZCCHC6 and ZCCHC11 have redundant RNA editing activity [21,31,40]. Importantly, while
167 *Zcchc11* heterozygotes exhibited slight reticulocytosis, this was not observed in
168 *Zcchc11* KOs, suggesting that Zcchc11 may provide at best partial redundancy
169 (Extended Data Fig. 7b). The *Zcchc6* and *Zcchc11* quad-flox system also showed that
170 significant reticulocytosis was observed only in animals with *Zcchc6* cKO (homozygous
171 floxed alleles of *Zcchc6* driven by *EpoR-Cre)*, but not in *Zcchc11* cKO (Extended Data
172 Fig. 8).
173

174 **Reticulocytosis showed postnatal attenuation.**

175 *Dis3l2* whole-body KO mice die shortly after birth, whereas *Dis3l2* cKOs under
176 *EpoR-Cre* survive postnatally, allowing us to investigate adult peripheral blood. Both
177 *Zcchc6 KO* and *Dis3l2* cKOs showed significant reticulocytosis at Postnatal day (P) 2
178 and P21 (Extended Data Fig. 9). Interestingly, the degree of reticulocytosis was
179 attenuated with age. We postulate there may be differential RNA regulation in the bone
180 marrow and adult peripheral blood compared to the embryonic spleen and blood.
181

182 **Characterization of accumulated RNA in *Zcchc6* and *Dis3l2* KO mice.**

183 Next, we investigated the nature of RNA accumulated in *Zcchc6* and *Dis3l2* KOs
184 at E18.5 utilizing RNA-seq (Fig. 3). The estimated expression levels in *Zcchc6* and
185 *Dis3l2* KOs clustered by KO genotype (Extended Data Fig. 10b). In PCA analysis, the
186 *Dis3l2* KO differed more from the WT than did the *Zcchc6* KO (Fig. 3b), consistent with
187 more severe RNA accumulation in *Dis3l2* KO than in *Zcchc6* KO. Differential gene
188 expression analysis also showed that *Dis3l2* KOs had more differentially expressed
189 transcripts than did the *Zcchc6* KOs (Fig. 3c). Both *Zcchc6* and *Dis3l2* KOs had more
190 over-represented transcripts (3.0% and 9.6%) than under-represented transcripts (1.3%
191 and 5.3%). Downregulated transcripts lacked any significant gene ontology

192 categories, suggesting a lack of target specificity for the population of affected mRNAs.
193 On the other hand, upregulated genes for each KO demonstrated some gene ontology
194 term enrichment. “Cytoplasmic translation” and “ribonucleoprotein complex
195 biogenesis” were the most enriched terms in *Zcchc6* KO, whereas enriched terms for
196 *Dis3l2* KO were “regulation of the mRNA metabolic process”, “proteasomal protein
197 catabolic process”, “NIK/NF-kappaB signaling”, “generation of precursor metabolites
198 and energy”, and “ribonucleoprotein complex subunit organization” (Extended Data Fig.
199 10c). When the differentially expressed genes from both KOs were overlaid (Fig. 3d),
200 we found that most genes (75% of the total) were aligned in the same regulatory
201 direction, with the majority being accumulated in both KOs. This included the non-
202 coding RNA *H19*, a known target of Dis3l2, identified in a previous nephron progenitor
203 study [41]. “Cytoplasmic translation” and “ribonucleoprotein complex regulation” were
204 gene ontology terms common to both KOs (Fig. 3e). We further validated the top
205 upregulated and downregulated genes by performing qPCRs on cKO samples (Fig. 3f).
206 The direction of regulation was consistent, with several genes significantly upregulated
207 in both cKOs: *Hbb-bh1*, *Ccnd3*, *Gnb2*, *Hspa8*, and *Alad*. The *Hbb-bh1* transcript was
208 more upregulated in the *Dis3l2* KO than in the *Zcchc6* KO, consistent with our
209 observation of greater RNA accumulation in the *Dis3l2* KO. *Hbb-bh1* is the
210 embryonic/fetal globin, which is unusual to observe at our dissection time point of
211 E18.5, as globin switching has already occurred in wild type mice by this point [42,43].
212

213 **Upregulation of *γ*-globin in *Zcchc6* and *Dis3l2* KOs in Humanized Mice.**

214 Hbb-bh1 is the ortholog of the human fetal γ-globin (gamma; *HBG1/HBG2*).
215 Research has established that patients with pathogenic sickle cell mutations in adult β-
216 globin show improved symptomology following reactivation of fetal γ-globin[25,44]. Thus,
217 we aimed to test whether *Zcchc6/Dis3l2* deficiency would upregulate the human γ-
218 globin gene. We crossed our *Zcchc6* and *Dis3l2* KOs with a humanized β-YAC model
219 mouse harboring the human β-globin gene cluster as a yeast artificial chromosome
220 transgene [45] (Fig. 4a) and validated the new model through genomic and protein
221 analysis (Extended Data Fig.11a, b). The human *γ*-globin was significantly
222 upregulated in erythroid cells at E18.5 in the *Zcchc6* and *Dis3l2* KOs (Fig. 4b). These

223 humanized β-YAC mice also preserved human globin switching in the mouse, enabling
224 the profiling of the dynamics of all β-like globins[45]. We examined erythroid cells at an
225 earlier time point (E14.5 fetal liver) and observed up-regulation of human fetal *γ*-
226 globins and down-regulation of adult *β*-globin relative to WT (Fig. 4c). At E18.5, this
227 pattern of reverse switching persisted in the peripheral blood, albeit to a lesser degree
228 (Fig. 4d), and was independent of maturation differences between KO and WT mice
229 (Extended Data Fig. 11 c&d). Together, these results highlight that ZCCHC6/DIS3L2
230 upregulates human fetal γ-globin in a conserved manner.
231

232 **Profiling ZCCHC/DIS3L2 during human *in vitro* erythropoiesis.**

233 Following our mouse studies, we adopted a human *in vitro* system for
234 erythropoiesis that enables a single, synchronized wave of differentiation, as
235 described[46], to allow detailed molecular studies. We performed *in vitro* erythropoiesis
236 with human umbilical cord blood-derived CD34+ cells and profiled protein expression
237 and globin mRNA expression (Extended Data Fig. 12). Flow cytometry profiles of
238 differentiating erythroid precursors from cord blood mirrored that of native erythroid
239 ontogeny, with expression of CD71, followed by glycophorin A, and ultimately
240 incomplete terminal loss of CD71 compared to adult peripheral blood (Extended Data
241 Fig. 12b). Immunoblotting showed increasing pan-hemoglobin levels through D20,
242 followed by decreased levels at D23 when some cell lysis occurs. DIS3L2 was highly
243 expressed starting on D9 and thereafter decreased, while ZCCHC6 was highly
244 expressed on D12 and D16, and decreased thereafter (Extended Data Fig. 12c).
245 Expression of mRNA for HBE (*ε*) and HBG1/2 (*γ*) increased until terminal stages when
246 levels dropped in the setting of cell lysis (Extended Data Fig. 12d). The expression of
247 HBB (β-globin) increased significantly until D16, after which it declined. Histological view
248 at D12 and D16 revealed that erythroid cells become extensively hemoglobinized and
249 exhibit highly condensed or absent nuclei (Extended Data Fig. 12e).
250

251 **CRISPR KOs during *in vitro* erythropoiesis phenocopy KO mice.**

252 Next, we used CRISPR/Cas9 to generate KOs by introducing ribonucleoprotein
253 complexes targeting ZCCHC6, DIS3L2, and the AAVS1 locus as a control (Fig. 5a) [47,48].

We conducted genomic analysis at D12 of differentiation, selected samples with over 60% frameshift indels, and confirmed significantly decreased protein levels (Extended Data Fig. 13a&b). KO of the RNA editing machinery did not impact maturation profiles, as reflected by flow cytometry for CD71 and GlyA (Extended Data Fig. 13c). However, we observed significant accumulation of RNA, as reflected by staining with TO (Fig. 5b). In both ZCCHC6 and DIS3L2 KOs, fetal *γ*-globin was upregulated while adult *β*-globin was relatively downregulated (Fig. 5c). However, the effect size was greater for KO of ZCCHC6 relative to DIS3L2. Taken together, these data demonstrate RNA accumulation in CRISPR knockout (KO) cells, which is consistent with the KO mice study, and a reversed globin-switching pattern in these cells, aligning with the humanized murine model study.

In vitro erythroid cells from PB with CRISPR KOs and HU treatment.

Reactivation or elevation of the expression of human fetal *γ*-globin by genetic or pharmacologic means is an effective therapeutic strategy in sickle cell disease and transfusion-dependent thalassemia [49]. Hydroxyurea (HU) treatment is known to elevate γ-globin levels in the peripheral blood of patients with hemoglobinopathies [50,51]. While a direct mechanistic connection between HU and ZCCHC6 has not been described, a previous study revealed that HU-induced DNA replication arrest triggers the rapid degradation of histone mRNA, mediated by uridylation from ZCCHC6 [52].

In this experiment, we aim to test whether the genetic deficiency of ZCCHC6/DIS3L2 affects PB (Peripheral Blood) HPSCs, which better reflect a clinical setting compared to CB HPSCs due to their low baseline levels of fetal hemoglobin. The PB CD34+ cells were subjected to CRISPR knockout (KO) of the RNA editing machinery and differentiated after day 9 in the absence or presence of HU (Fig. 6a) [53,54]. Consistently, accumulation of reticulocytes (GlyA+CD71^{low}TO^{high} cells), elevation of γ-globin levels, and reversed switching patterns were noted in ZCCHC6 CRISPR KOs (Fig. 6b, c, d), while DIS3L2 CRISPR KOs showed a similar trend with a marginal p-value for the first two features. Upon DIS3L2 CRISPR KOs, adult β-globin was also upregulated, resulting in our inability to observe reverse-switching. Genomic analysis at day 12 demonstrated similar frame-shift editing rates in both PB and CB CD34+ cells.

285 No differential impact on erythroid maturation profiles were observed upon CRISPR
286 KOs and HU treatment (Extended Data Fig. 14a & b).
287 When compared with HU treatment, KO of ZCCHC6 alone showed better
288 upregulation of γ-globin levels and reverse switching between γ and β globins than HU
289 treatment (Fig. 6c &d). Furthermore, HU treatment did not augment the impact, likely
290 because the cells reached the maximum capacity to carry fetal globin. Taken together,
291 these results highlight that ZCCHC6 is a consistent regulator in both CB and PB-derived
292 cells. Our data implicating ZCCHC6 as a regulator of γ-globin mRNA stabilization
293 suggests that ZCCHC6 may be a target worth testing further as a therapeutic strategy
294 for enhancing γ-globin expression in hemoglobinopathies.
295

296 **DISCUSSION**

297 During terminal differentiation, erythroid cells dramatically discard cellular
298 components, including the nucleus, mitochondria, and ribosomes[3–7]. Nuclear
299 condensation and enucleation entail a loss of transcription[1,3,4], implicating post-
300 transcriptional regulatory mechanisms as prominent drivers of transcriptome shedding.
301 The resulting transcriptome, with its low-entropy, globin-rich composition in terminal
302 erythroid cells, is thought to be achieved by the active decay of RNAs that are
303 nonessential for mature RBC function[9,10]. However, the exact molecular pathways
304 driving this process have not been elucidated. In this study, we discovered that the
305 ZCCHC6-DIS3L2 RNA editing pathway plays a role in RNA shedding during terminal
306 erythropoiesis, with a prominent target for degradation being fetal (γ-) hemoglobin. Our
307 finding complements the previous discovery of global proteome shedding through
308 ubiquitination[11], as both mechanisms involve post-translational and post-transcriptional
309 tagging, respectively, to target molecules for degradation. Our finding begs the question
310 of how β-globin mRNA escapes this shedding process. Previous studies have shown
311 that pyrimidine-rich cis-elements in the 3' UTR, along with associated trans-elements
312 such as αCP and nucleolin, stabilize β-globin mRNAs [55,56]. This RNP complex may
313 outcompete ZCCHC6 or form an untaggable substrate for the ZCCHC6-DIS3L2
314 pathway.

315 Hereditary Persistence of Fetal Hemoglobin (HPFH), a benign genetic condition
316 manifesting as incomplete globin switching, mediates significant amelioration of
317 symptoms when inherited along with the genetic mutation in Sickle Cell Disease
318 (SCD)[25]. This experiment of nature has inspired a therapeutic strategy to reactivate fetal
319 γ-globin via genetic perturbation of the γ-globin repressor BCL11A, resulting in
320 transcriptional reactivation and considerable clinical improvement for SCD
321 patients[44,49,57,58]. Reactivation of γ-globin by genetic editing has achieved proof of
322 concept for treating hemoglobinopathies, marking a seminal translational application of
323 gene editing technology [44,49]. However, it is challenging to deliver genetic therapy for
324 SCD patients in under-resourced areas of the globe, where SCD is most prevalent [59,60].
325 This challenge arises from the scarcity of bone marrow transplantation centers and
326 trained healthcare providers[59,60], and by the high costs of genetic therapies[61]. The
327 development of small molecule inhibitors that can reactivate γ-globin expression,
328 including inhibition of BCL11A, remains an appealing alternative that could be more
329 readily distributed in under-resourced locales[62–66]. However, achieving therapeutic
330 levels of γ-globin reactivation with a single drug has, to date, proven challenging due to
331 the suboptimal potency of monotherapy and heterogenous pathological symptoms[65].
332 The successful treatment may therefore require the use of multiple pharmacological
333 agents[65].
334 Here, we report a novel post-transcriptional mechanism whereby γ-globin mRNA
335 is subject to active degradation. This discovery raises the possibility that therapeutic
336 strategies to stabilize γ-globin mRNA could synergize with pharmacologic strategies that
337 reactivate γ-globin mRNA expression to ameliorate the symptoms and deleterious
338 health consequences of hemoglobinopathies. Recent studies have reported small
339 molecule activators of γ-globin expression[65,66], as well as inhibitors of ZCCHC6/11
340 which have been developed as anti-cancer agents[67,68]. In the latter case, inhibitors
341 reduced the uridylation of target RNAs, including *pre-let-7*[67], and demonstrated
342 antiproliferative activity in focadhesin (FOCAD)-deleted cancer[68]. Testing existing
343 ZCCHC6 inhibitors or developing novel inhibitors using assays with γ-globin RNA as a
344 substrate in erythroid cells could offer an accessible pharmacological option.

345 While we observed delayed globin switching, prolonged γ-globin mRNA half-life,
346 reticulocytosis and anemia in the embryonic circulation of *Zcchc6* and *Dis3l2* KO mice,
347 these phenotypes were attenuated in post-weanling mice, when fetal erythropoiesis is
348 fully extinguished in favor of adult patterns of red cell development. Resculpting of the
349 terminal transcriptome during adult murine erythropoiesis most likely entails an additive
350 or distinct regulatory mechanism. In our *in vitro* studies of human erythropoiesis from
351 adult peripheral blood, we observed modest stabilization of γ-globin mRNA by ZCCHC6
352 knock-out, suggesting that the ZCCHC6 machinery is active in adult erythropoiesis.
353 Strategies to reactivate and stabilize γ-globin in adult red blood cells remains to be
354 further optimized.
355 Akin to human β-globins, human α-globin mRNAs are selectively stabilized
356 during terminal erythropoiesis, by a mechanism that entails binding of the αCP complex
357 at polypyrimidine-rich sites within the 3' UTR [69]. In $\alpha^{\text{Constant Spring (CS)}}$ thalassemia,
358 mutation of the 3' UTR disrupts αCP complex formation, leading to accelerated mRNA
359 decay, characterized by shortened poly(A) tails [70]. Upon *Zcchc6* KO (but not in *Dis3l2*
360 KO), RNA-seq results show that the embryonic α-like ζ-globin gene (*Hba-x*) was
361 significantly upregulated in terminal erythroid cells at E18.5. It is therefore likely that ζ-
362 globin and *γ*-globin share the RNA editing machinery that regulates their mRNA stability
363 post-transcriptionally, most notably ZCCHC6, warranting future studies to investigate
364 the consequences of ZCCHC6 KO in $\alpha^{\text{Constant Spring (CS)}}$ thalassemia.
365

366 # METHODS

367 ## Animal Models

368 All experiments were performed with previously reported KO models for *Lin28a*
369 and *Lin28b*, as well as KO and flox lines for *Zcchc6* and *Zcchc11*[13,71,72]. Whole body and
370 conditional *Dis3l2* KO mice were generated in-house as follows: Targeted mESCs
371 ($\text{Dis3l2}^{\text{tm1a(EUCOMM)Hmgu}}$) were obtained from Helmholtz Zentrum München via the
372 European Conditional Mouse Mutagenesis Program (EUCOMM)[73]. The gene-targeted
373 ESCs were injected into chimeric blastocysts. Once injected, they were implanted into
374 pseudopregnant Balb/c females and mutant mice were established. To ascertain
375 germline transmission, we crossed chimeras to WT mice, screened the offspring, and

376 obtained several Dis3l2 transgenic animals with germline transmission, after which the
377 strain was expanded. Constitutive knockout of Dis3l2 was generated by crossing
378 females carrying *Vasa-Cre* allele (Jackson laboratory, stock #006954) to *Dis3l2*
379 transgenic males. The cross resulted in the constitutive deletion of Dis3l2 in all tissues
380 by virtue of *Cre* expression in oocytes[74]. Conditional *Dis3l2* flox line was generated by
381 crossing *Dis3l2* transgenic mice to Actin-Flippase (Flp) first (B6.Cg-
382 Tg(ACTFLPe)9205Dym/J, the Jackson Laboratory Strain #005703) to remove Lac-Z
383 reporter cassette, followed by *Cre* breeding.
384 The *Zcchc6* and *Dis3l2* flox animals were crossed with previously published
385 *EpoR-Cre* mice to generate an erythroid-specific conditional KO mouse [38]. Humanized
386 beta-globin YAC mice were bred with *Zcchc6/Dis3l2* KO mice [45]. Embryonic and adult
387 ear tissue genotyping was performed either manually or automatically (using
388 Transnetyx) to confirm the genotypes of KO, flox, and humanized lines. Conditional
389 *Zcchc6* and *Dis3l2* KOs in the newly generated murine models were validated by
390 western blots (1:1000 for both antibodies, α-ZCCHC6; Protein Tech 25196-1-AP and α-
391 DIS3l2; NBP1-84740) on the sorted erythroid cells (PI-Hoechst-TER119+ cells). Animal
392 experiments were performed by protocols approved by the Institutional Animal Care and
393 Use Committee at Boston Children's Hospital.
394

395 **Murine Blood/Tissue Collection and Analysis**

396 Embryonic blood was collected from embryos harvested via Caesarian section.
397 Blood of postnatal and adult mice was harvested through tail clipping or retro-orbital
398 bleeding. During time-series analysis across various developmental ages, we bled each
399 animal only once to avoid reticulocytosis secondary to anemia. Blood was collected
400 using heparinized capillary tubes into EDTA-coated collection tubes, then subsequently
401 processed using a HEMAVET machine and Fluorescence-Activated Single Cell Sorting
402 (FACS) profiling.
403 One ul of blood was diluted into 50 ul of a buffered saline citrate glucose solution
404 (BSCG) and mixed with equal parts of staining buffer (PBS + 2% serum + 1X pen/strep)
405 containing a 1:100 dilution of each antibody: TER119 (BD Pharmingen 557909), CD71
406 (BD Clone: C2), Thiazole Orange (Sigma-Aldrich-390062), Hoechst 33342 (Invitrogen

407 R37165), and Propidium Iodide (BD Pharmingen 51-66211E). All acquisition was
408 performed on an LSR/FORTESSA cytometer, and the results were analyzed using
409 FlowJo and Prism software. Spleen and liver cells were dissociated in ice-cold PBS,
410 filtered, and then subjected to FACS analysis using the same staining panel.
411 For hemolytic marker assays, we collected plasma and serum samples,
412 incubating the latter at room temperature for 30 minutes to allow for coagulation. We
413 performed centrifugation at 1,500x g for 10 minutes at 4°C and collected plasma and
414 serum samples for downstream analysis (western blots and blood biochemistry assays).
415 The plasma was then mixed and heated in a protein preparation solution (RIPA buffer
416 with protease and phosphatase inhibitors, and DTT). The protein samples were
417 loaded onto Bis-Tris gels, and the transferred membranes were probed with primary
418 antibodies (1:500 and 1:1000 for each antibody respectively: α-Haptoglobin; Life
419 Technologies # 16665-1-AP and α-IgG; ab190475). LDH (Abcam no. ab102526) and
420 bilirubin (Sigma Aldrich # MAK126) assays were performed according to the
421 manufacturers' instructions. The LDH samples were harvested from heparin-coated
422 collection tubes instead of the EDTA-coated tubes.
423

424 **Blood Histology**

425 Blood smears were prepared on frosted slides and stained with May-Grünwald
426 and Giemsa solutions (Sigma-Aldrich; MG500 and GS500). The slides were placed in
427 the May-Grünwald solution for two minutes, then were subsequently incubated in a
428 diluted Giemsa solution (1:25 with milliQ H_2O) for 12 minutes and washed with
429 autoclaved Milli-Q H_2O. Reticulocytes were identified using methylene blue staining
430 protocol (Sigma-Aldrich; R4132). The stained slides were coated (VECTASHIELD) and
431 examined under a microscope.
432

433 **Transcriptomic (RNA-seq) and Transcript Analysis (RT-qPCRs)**

434 Enucleated erythroid cells ($PI^-Hoechst^-TER119^+$ cells) were sorted directly into
435 concentrated TRIzol (TRIzol™ LS Reagent). Total RNA was isolated using a column
436 assay with DNase treatment (Direct-zol MicroPrep, ZYMO). The quantity and quality of
437 RNA were evaluated using a nanodrop machine and RNA screen tape. We constructed

438 an RNA-seq library with high-quality RNA (Both 260/280 and 260/230 over 1.7 with
439 RNA integrity number >7) after ribosomal RNA depletion. For regular gene expression
440 analysis, adapter-trimmed reads from the sequencer were mapped to the mouse
441 genome, quantified, and analyzed using seq data analysis tools (Cutadapt, Bowtie,
442 TopHat, HTSeq, R, and edgeR). For RT-qPCRs, cDNA was reverse transcribed from
443 the isolated RNA (using the Maxima First Strand cDNA Synthesis Kit, Thermo Fisher
444 Scientific). Then, quantitative PCR (qPCR) was performed using either SYBR Green or
445 TaqMan assays (on a QuantStudio machine, Applied Biosystems).
446

447 **Human *In vitro* Erythropoiesis from Hematopoietic Stem/Progenitor Cells**

448 Hematopoietic stem and progenitor (CD34+ HSPCs) cells derived from umbilical
449 cord blood or adult peripheral blood were purchased (mixed donor vials,
450 ALLCELLS/STEMCELL technologies) and subjected to the *in vitro* RBC differentiation
451 protocol described in the previous study [46]. Genetic KOs were generated in CD34+
452 HSPCs via nucleofection of CRISPR/Cas9 ribonucleoproteins (RNPs)[48]. First, CD34+
453 cells were thawed dropwise and cultured for two days before nucleofection in SFEM II
454 media (StemCell Technologies, 09605) supplemented with 100 ng/mL SCF, TPO,
455 FLT3L, and IL-6. The CD34+ HSPCs were nucleofected with Cas9 RNPs (125 pmol of
456 sgRNA complexed with 105 pmol of Cas9 protein) using a Lonza 4D-Nucleofector. Cells
457 were subsequently cultured for recovery and expansion, followed by the initiation of *in*
458 *vitro* differentiation assays, and then harvested for genomic DNA extraction using a lysis
459 buffer. The gRNA-targeted genomic loci (~200 bp flanking regions of the expected Cas9
460 cut site) were PCR-amplified, gel-purified, and sanger-sequenced. The frameshifting
461 Indel frequencies for each gRNA were quantified using TIDE analysis (http://tide.nki.nl).
462 Hydroxyurea (Sigma) was purchased, freshly resuspended in ultra-pure water each
463 time, and added to the cell cultures. For downstream qPCR analysis, cells were washed
464 twice with ice-cold PBS, lysed in TRIzol, and their cDNAs were subsequently subjected
465 to qPCRs. For Western blot and FACS analysis, we used the same method described in
466 the murine sample analysis, except for the use of specific human antibodies:
467 Hemoglobin β/γ/δ/ε Antibody (sc-390668) for western blot, and anti-Human CD71

(Fisher Scientific, BDB555537) and GlyA (CD235a, Beckman Coulter, A71564) for FACS analysis.

Statistical Analysis

Data are expressed as mean ± SD. For hematological profile analysis, adjusted p-values were calculated from a linear mixed-effects model adjusted for sex (fixed effect) and litter information (random effect), followed by post-hoc multiple pairwise comparisons based on Tukey's Honest Significant Difference (HSD) adjustment. For all other analyses, p-values were calculated using t-tests (* <0.05, ** <0.01, *** <0.001, **** <0.0001).

Data availability

The resulting RNA-seq data is available on the Gene Expression Omnibus (GEO) database (GSE151184).

Code availability

All scripts and codes are available upon request.

REFERENCES

1. Dzierzak, E. & Philipsen, S. Erythropoiesis : Development and Differentiation. (2013).
2. Palis, J. Primitive and definitive erythropoiesis in mammals. *Front Physiol* **5 JAN**, 1–9 (2014).
3. Keerthivasan, G., Wickrema, A. & Crispino, J. D. Erythroblast enucleation. *Stem Cells Int* **2011**, (2011).
4. Menon, V. & Ghaffari, S. Erythroid enucleation: a gateway into a “bloody” world. *Exp Hematol* **95**, 13–22 (2021).
5. Moras, M., Lefevre, S. D. & Ostuni, M. A. From erythroblasts to mature red blood cells: Organelle clearance in mammals. *Front Physiol* **8**, 1–9 (2017).
6. Kundu, M. *et al.* Ulk1 plays a critical role in the autophagic clearance of mitochondria and ribosomes during reticulocyte maturation. *Blood* **112**, 1493–1502 (2008).
7. Schweers, R. L. *et al.* NIX is required for programmed mitochondrial clearance during reticulocyte maturation. *Proc Natl Acad Sci U S A* **104**, 19500–19505 (2007).
8. Ovchynnikova, E., Aglialoro, F., von Lindern, M. & van den Akker, E. The shape shifting story of reticulocyte maturation. *Front Physiol* **9**, 1–14 (2018).
9. Bastos, R. N. & Aviv, H. Theoretical analysis of a model for globin messenger RNA accumulation during erythropoiesis. *J Mol Biol* **110**, 205–218 (1977).

504 10. Bastos, R. N., Volloch, Z. & Aviv, H. Messenger RNA population analysis during
505 erythroid differentiation: A kinetical approach. *J Mol Biol* **110**, 191–203 (1977).
506 11. Nguyen, A. T. *et al.* UBE2O remodels the proteome during terminal erythroid
507 differentiation. *Science* **357**, (2017).
508 12. Thomas, M. P. *et al.* Apoptosis Triggers Specific, Rapid, and Global mRNA Decay with
509 3' Uridylated Intermediates Degraded by DIS3L2. *Cell Rep* **11**, 1079–1089 (2015).
510 13. Morgan, M. *et al.* MRNA 3′ uridylation and poly(A) tail length sculpt the mammalian
511 maternal transcriptome. *Nature* **548**, 347–351 (2017).
512 14. Kozlowski, E. *et al.* The RNA uridyltransferase Zcchc6 is expressed in macrophages and
513 impacts innate immune responses. *PLoS One* **12**, 1–16 (2017).
514 15. Ansari, M. Y. *et al.* Genetic Inactivation of ZCCHC6 Suppresses Interleukin-6 Expression
515 and Reduces the Severity of Experimental Osteoarthritis in Mice. *Arthritis Rheumatol* **71**,
516 583–593 (2019).
517 16. Lin, C. C. *et al.* Terminal uridyltransferase 7 regulates TLR4-triggered inflammation by
518 controlling Regnase-1 mRNA uridylation and degradation. *Nat Commun* **12**, (2021).
519 17. Gupta, A. *et al.* TUT4/7-mediated uridylation of a coronavirus subgenomic RNAs delays
520 viral replication. *Commun Biol* **6**, 1–9 (2023).
521 18. Lee, M., Kim, B. & Kim, V. N. Emerging roles of RNA modification: M6A and U-Tail.
522 *Cell* **158**, 980–987 (2014).
523 19. Lackey, P. E., Welch, J. D. & Marzluff, W. F. TUT7 catalyzes the uridylation of the 3′
524 end for rapid degradation of histone mRNA. *Rna* **22**, 1673–1688 (2016).
525 20. Le Pen, J. *et al.* Terminal uridylyltransferases target RNA viruses as part of the innate
526 immune system. *Nat Struct Mol Biol* **25**, 778–786 (2018).
527 21. Lim, J. *et al.* Uridylation by TUT4 and TUT7 Marks mRNA for Degradation. *Cell* **159**,
528 1365–1376 (2014).
529 22. Chang, H. *et al.* Terminal Uridylyltransferases Execute Programmed Clearance of
530 Maternal Transcriptome in Vertebrate Embryos. *Mol Cell* **70**, 72-82.e7 (2018).
531 23. Barbarani, G., Labedz, A., Stucchi, S., Abbiati, A. & Ronchi, A. E. Physiological and
532 Aberrant γ-Globin Transcription During Development. *Front Cell Dev Biol* **9**, 1–10
533 (2021).
534 24. Wienert, B., Martyn, G. E., Funnell, A. P. W., Quinlan, K. G. R. & Crossley, M. Wake-up
535 Sleepy Gene: Reactivating Fetal Globin for β-Hemoglobinopathies. *Trends in Genetics*
536 **34**, 927–940 (2018).
537 25. Akinsheye, I. *et al.* Fetal hemoglobin in sickle cell anemia. *Blood* **118**, 19–27 (2011).
538 26. Blobel, G. A. & Khandros, E. Elevating fetal hemoglobin - recently discovered regulators
539 and mechanisms. *Blood Journal* (2024) doi:10.1182/blood.2023022190.
540 27. Lu, H. Y., Orkin, S. H. & Sankaran, V. G. Fetal Hemoglobin Regulation in Beta-
541 Thalassemia. *Hematol Oncol Clin North Am* **37**, 301–312 (2023).
542 28. Elagooz, R. *et al.* PUM1 mediates the posttranscriptional regulation of human fetal
543 hemoglobin. *Blood Adv* **6**, 6016–6022 (2022).
544 29. Wakabayashi, A. *et al.* Identification and characterization of RBM12 as a novel regulator
545 of fetal hemoglobin expression. *Blood Adv* **6**, 5956–5968 (2022).
546 30. Faehnle, C. R., Walleshauser, J. & Joshua-Tor, L. Mechanism of Dis3l2 substrate
547 recognition in the Lin28-let-7 pathway. *Nature* **514**, 252–256 (2014).
548 31. Pirouz, M., Du, P., Munafò, M. & Gregory, R. I. Dis3l2-Mediated Decay Is a Quality
549 Control Pathway for Noncoding RNAs. *Cell Rep* **16**, 1861–1873 (2016).

550 32. Mosqueira, M., Willmann, G., Zeiger, U. & Khurana, T. S. Expression profiling reveals
551 novel hypoxic biomarkers in peripheral blood of adult mice exposed to chronic hypoxia.
552 *PLoS One* **7**, 1–10 (2012).
553 33. Palis, J. Ontogeny of erythropoiesis. *Curr Opin Hematol* **15**, 155–161 (2008).
554 34. Kingsley, P. D. *et al.* Ontogeny of erythroid gene expression. *Blood* **121**, 5–13 (2013).
555 35. Lee, L. G., Chen, C. H. & Chiu, L. A. Thiazole orange: a new dye for reticulocyte
556 analysis. *Cytometry* **7**, 508–517 (1986).
557 36. Malleret, B. *et al.* Plasmodium vivax: Restricted tropism and rapid remodeling of CD71-
558 positive reticulocytes. *Blood* **125**, 1314–1324 (2015).
559 37. Yumine, A., Fraser, S. T. & Sugiyama, D. Regulation of the embryonic erythropoietic
560 niche: A future perspective. *Blood Res* **52**, 10–17 (2017).
561 38. Heinrich, A. C., Pelanda, R. & Klingmüller, U. A mouse model for visualization and
562 conditional mutations in the erythroid lineage. *Blood* **104**, 659–666 (2004).
563 39. Barcellini, W. & Fattizzo, B. Clinical Applications of Hemolytic Markers in the
564 Differential Diagnosis and Management of Hemolytic Anemia. *Dis Markers* **2015**, (2015).
565 40. Thornton, J. E., Chang, H.-M., Piskounova, E. & Gregory, R. I. Lin28-mediated control of
566 let-7 microRNA expression by alternative TUTases Zcchc11 (TUT4) and Zcchc6 (TUT7).
567 *RNA* vol. 18 1875–1885 Preprint at https://doi.org/10.1261/rna.034538.112 (2012).
568 41. Hunter, R. W. *et al.* Loss of Dis3l2 partially phenocopies perlman syndrome in mice and
569 results in upregulation of Igf2 in nephron progenitor cells. *Genes Dev* **32**, 903–908 (2018).
570 42. Sankaran, V. G., Xu, J. & Orkin, S. H. Advances in the understanding of haemoglobin
571 switching: Review. *Br J Haematol* **149**, 181–194 (2010).
572 43. McGrath, K. E. *et al.* A transient definitive erythroid lineage with unique regulation of the
573 β-globin locus in the mammalian embryo. *Blood* **117**, 4600–4608 (2011).
574 44. Orkin, S. H. & Bauer, D. E. Emerging Genetic Therapy for Sickle Cell Disease. *Annu Rev*
575 *Med* **70**, 257–271 (2019).
576 45. Porcu, S. *et al.* The human β globin locus introduced by YAC transfer exhibits a specific
577 and reproducible pattern of developmental regulation in transgenic mice. *Blood* **90**, 4602–
578 4609 (1997).
579 46. Huang, N. J. *et al.* Genetically engineered red cells expressing single domain camelid
580 antibodies confer long-Term protection against botulinum neurotoxin. *Nat Commun* **8**, 1–
581 13 (2017).
582 47. Bak, R. O., Dever, D. P. & Porteus, M. H. CRISPR/Cas9 genome editing in human
583 hematopoietic stem cells. *Nat Protoc* **13**, 358–376 (2018).
584 48. Sanson, K. R. *et al.* Optimized libraries for CRISPR-Cas9 genetic screens with multiple
585 modalities. *Nat Commun* **9**, 1–15 (2018).
586 49. Daley, G. Q. Welcoming the Era of Gene Editing in Medicine. *N Engl J Med* **390**, 1642–
587 1645 (2024).
588 50. Rodgers, G. P., Dover, G. J., Noguchi, C. T., Schechter, A. N. & Nienhuis, A. W.
589 Hematologic responses of patients with sickle cell disease to treatment with hydroxyurea.
590 *N Engl J Med* **322**, 1037–1045 (1990).
591 51. Platt, O. S. *et al.* Hydroxyurea enhances fetal hemoglobin production in sickle cell
592 anemia. *J Clin Invest* **74**, 652–656 (1984).
593 52. Holmquist, C. E., He, W., Meganck, R. M. & Marzluff, W. F. Erratum: Knockouts of
594 TUT7 and 3′hExo show that they cooperate in histone mRNA maintenance and

595 degradation (RNA (2022) 28 (1519–1533) DOI: 10.1261/rna.079233.122). *Rna* **29**, 862
596 (2023).
597 53. Zhu, X. *et al.* Hydroxyurea differentially modulates activator and repressors of γ-globin
598 gene in erythroblasts of responsive and non-responsive patients with sickle cell disease in
599 correlation with Index of Hydroxyurea Responsiveness. *Haematologica* **102**, 1995–2004
600 (2017).
601 54. Cokic, V. P. *et al.* Hydroxyurea induces fetal hemoglobin by the nitric oxide–dependent
602 activation of soluble guanylyl cyclase. *Journal of Clinical Investigation* **111**, 231–239
603 (2003).
604 55. Jiang, Y., Xu, X.-S. & Russell, J. E. A Nucleolin-Binding 3′ Untranslated Region Element
605 Stabilizes β-Globin mRNA In Vivo. *Mol Cell Biol* **26**, 2419–2429 (2006).
606 56. Yu, J. & Russell, J. E. Structural and Functional Analysis of an mRNP Complex That
607 Mediates the High Stability of Human β-Globin mRNA. *Mol Cell Biol* **21**, 5879–5888
608 (2001).
609 57. Xu, J. *et al.* Correction of sickle cell disease in adult mice by interference with fetal
610 hemoglobin silencing. *Science (1979)* **334**, 993–996 (2011).
611 58. Sankaran, V. G. *et al.* Developmental and species-divergent globin switching are driven
612 by BCL11A. *Nature* **460**, 1093–1097 (2009).
613 59. Kumar, A. & Bhattacharya, S. Sickle cell disease: a comparative perspective on global
614 and national initiatives. *Frontiers in Hematology* **3**, 1–6 (2024).
615 60. John, T. D., Namazzi, R., Chirande, L. & Tubman, V. N. Global perspectives on cellular
616 therapy for children with sickle cell disease. *Curr Opin Hematol* **29**, 275–280 (2022).
617 61. Basu, A. *et al.* Sickle Cell Disease in the United States : **177**, 155–164 (2024).
618 62. Zheng, G. *et al.* A tetramer of BCL11A is required for stable protein production and fetal
619 hemoglobin silencing. *Science* **386**, 1010–1018 (2024).
620 63. Saunthararajah, Y. Targeting sickle cell disease root-cause pathophysiology with small
621 molecules. *Haematologica* **104**, 1720–1730 (2019).
622 64. Takase, S. *et al.* A specific G9a inhibitor unveils BGLT3 lncRNA as a universal mediator
623 of chemically induced fetal globin gene expression. *Nat Commun* **14**, 1–18 (2023).
624 65. Telen, M. J., Malik, P. & Vercellotti, G. M. Therapeutic strategies for sickle cell disease:
625 towards a multi-agent approach. *Nat Rev Drug Discov* **18**, 139–158 (2019).
626 66. Ting, P. Y. *et al.* A molecular glue degrader of the WIZ transcription factor for fetal
627 hemoglobin induction. *Science* **385**, 91–99 (2024).
628 67. Lin, S. & Gregory, R. I. Identification of small molecule inhibitors of Zcchc11 TUTase
629 activity. *RNA Biol* **12**, 792–800 (2015).
630 68. Triboulet, R. *et al.* Targeting the synthetic lethal relationship between FOCAD and TUT7
631 represents a potential therapeutic opportunity for TUT4/7 small molecule inhibitors in
632 cancer. *Mol Cancer Ther* 1779–1788 (2024) doi:10.1158/1535-7163.mct-24-0176.
633 69. Russell, J. E., Morales, J. & Liebhaber, S. A. *The Role of MRNA Stability in the Control of*
634 *Globin Gene Expression. Progress in nucleic acid research and molecular biology* vol. 57
635 (Elsevier Masson SAS, 1997).
636 70. Morales, J., Russell, J. E. & Liebhaber, S. A. Destabilization of human α-globin mRNA
637 by translation anti-termination is controlled during erythroid differentiation and is
638 paralleled by phased shortening of the poly(A) tail. *Journal of Biological Chemistry* **272**,
639 6607–6613 (1997).

71. Osborne, J. K. *et al.* Lin28 paralogs regulate lung branching morphogenesis. *Cell Rep* **36**, 109408 (2021).
72. Yermalovich, A. V. *et al.* Lin28 and let-7 regulate the timing of cessation of murine nephrogenesis. *Nat Commun* **10**, (2019).
73. Skarnes, W. C. *et al.* A conditional knockout resource for the genome-wide study of mouse gene function. *Nature* **474**, 337–344 (2011).
74. Gallardo, T., Shirley, L., John, G. B. & Castrillon, D. H. Generation of a germ cell-specific mouse transgenic Cre line, Vasa-Cre. *Genesis (United States)* **45**, 413–417 (2007).
75. Kingsley, P. D. *et al.* Ontogeny of erythroid gene expression. *Blood* **121**, 5–13 (2013).

Acknowledgements

The authors would like to thank Dr. Ursula Klingmüller for granting permission to use the *EpoR-cre* mouse model; Dr. Susanna Porcu for permission to use the Human *β-Globin YAC* mouse model; Dr. Dónal O'Carroll for sharing the *Zcchc6* and *Zcchc11* whole-body and conditional knockout mouse models; Dr. Vijay Sankaran for providing the globin primer lists and engaging in scientific discussions; current and former members of the Daley, Thorsten, and North labs for valuable discussions and technical assistance; the Harvard Medical School Biopolymers Facility for sequencing; and the Research Computing Group for providing the O2 High-Performance Compute Cluster. This work was supported by PCTC (Progenitor Cell Translational Consortium; NHLBI UO1-HL134812) and T32 grants from the National Heart, Lung, and Blood Institute (NHLBI), U54DK110805: A Center of Molecular Hematology from National Institute of Diabetes and Digestive and Kidney Diseases (NIDDK), as well as an early career grant from the National Blood Foundation.

Author contributions

A.H. conceived the research question, performed experiments, and wrote the manuscript. A.Y. designed and conducted the Dis3l2 mice experiments. M.A.T.N. performed CRISPR/Cas9 knockouts and analyzed genome editing data. D.P. designed and established the ZCCHC6/11 mice study. Y.F. performed the blastocyst injections for the Dis3l2 study and guided the EpoR-cre and YAC mice studies. M.B. conducted mouse genotyping and RNA experiments. C.K. designed and provided guidance on FACS profiling. T.N. advised on the study. V.L. set up the human *in vitro* erythropoiesis

674 study and revised the manuscript. S.O. designed the EpoR-cre and YAC mice studies
675 and advised on the study. G.Q.D. conceived the idea, supervised the study, and wrote
676 the manuscript.

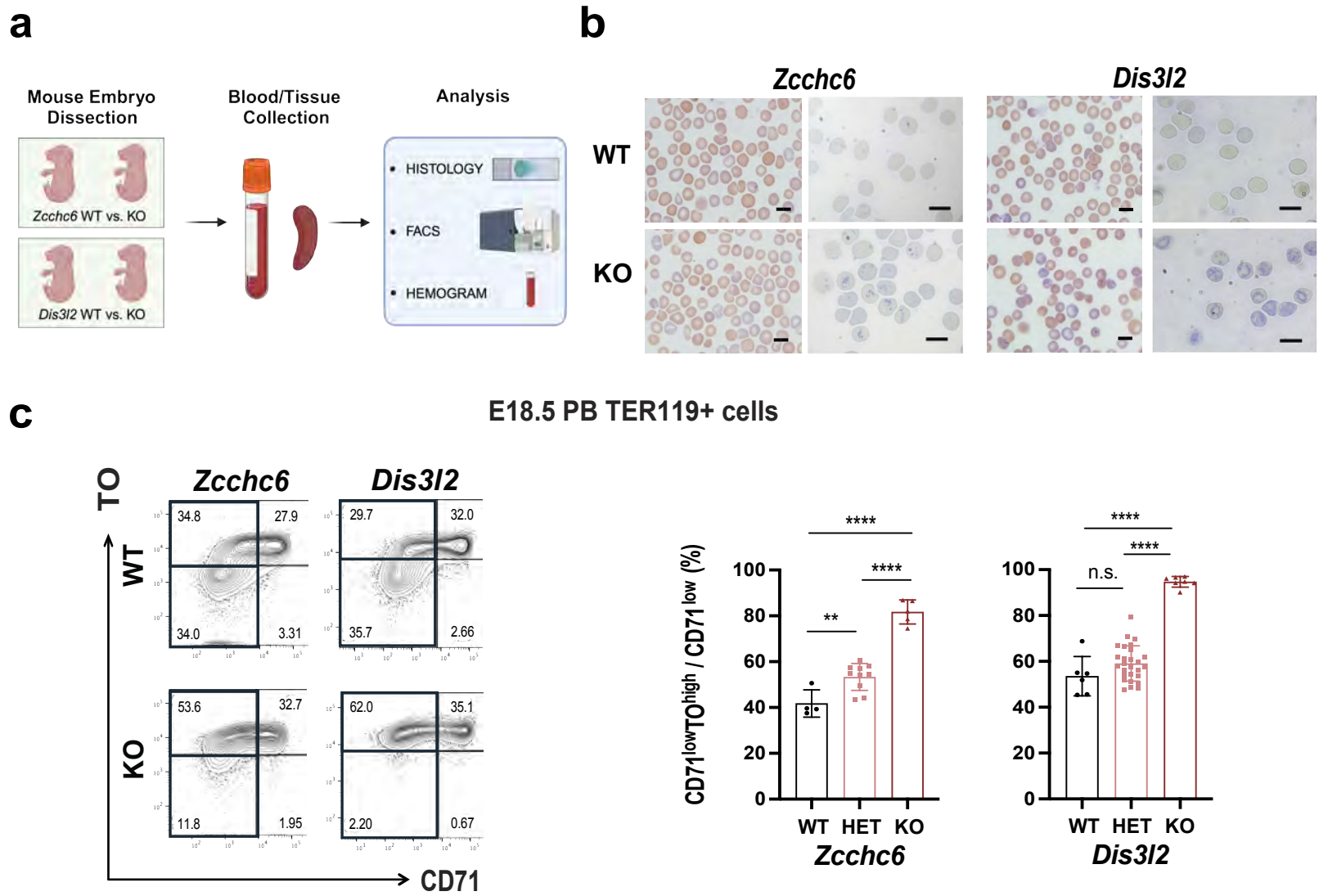

d

p-values (<0.05 *, <0.01 **, <0.001***)

Parameter	Unit	*Zcchc6*			p-value		*Dis3l2*			p-value	
		WT	HET	KO	WT vs. KO	HET vs. KO	WT	HET	KO	WT vs. KO	HET vs.KO
RBC	M/µl	3.06 ± 0.26	3.05 ± 0.14	2.73 ± 0.30	**	**	3.38 ± 0.34	3.49 ± 0.32	2.44 ± 0.34	***	***
HCT	%	44.18 ± 4.21	44.14 ± 3.46	40.00 ± 3.59	*	*	42.88 ± 4.17	44.31 ± 4.24	34.52 ± 2.93	***	***
MCH	pg	33.61 ± 1.87	33.68 ± 2.20	36.30 ± 2.09	**	**	32.42 ± 1.46	32.78 ± 1.57	35.25 ± 1.72	**	**
MCHC	g/dL	23.25 ± 0.98	23.30 ± 1.21	24.75 ± 1.31		*	25.62 ± 2.00	25.81 ± 0.92	25.62 ± 1.05		
MCV	fL	144.55 ± 4.43	144.62 ± 6.51	146.90 ± 9.88			126.98 ± 5.74	127.10 ± 6.46	137.85 ± 7.7	**	***
RDW	%	19.56 ± 0.53	19.06 ± 0.66	19.89 ± 0.32	*	***	17.82 ± 0.33	17.91 ± 0.81	18.82 ± 0.79		**
Hb	g/dL	10.26 ± 0.95	10.28 ± 0.91	9.90 ± 1.05			10.96 ± 1.15	11.44 ± 1.23	8.65 ± 1.02	***	***

Fig. 1. Analysis of Whole-Body *Zcchc6/Dis3l2* Knockout Mice.
(a) The overall scheme of the embryonic blood studies on *Zcchc6* and *Dis3l2* knockout (KO) mice.
(b) Histology of peripheral blood smears stained by May-Grünwald-Giemsa (left) and methylene blue (right). Scale bar = *10um*.
(c, left figure) Flow cytometry profiles of erythroid cells from peripheral blood (PB). Representative profiles of each KO and littermate WT were displayed.
(c, right graphs) Quantification of reticulocyte population per genotype (mean ± SD). Multiple litters were used.
(d) Hematological profiles of the peripheral blood (mean ± SD).
HCT; Hematocrit, MCH; Mean corpuscular hemoglobin, MCHC; Mean corpuscular hemoglobin concentration, MCV; Mean corpuscular volume, RDW; Red cell Distribution Width.

a

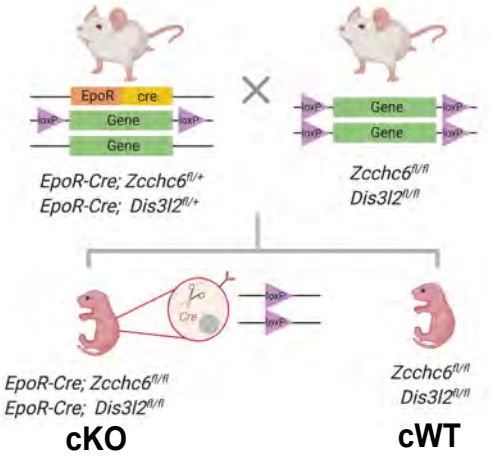

b

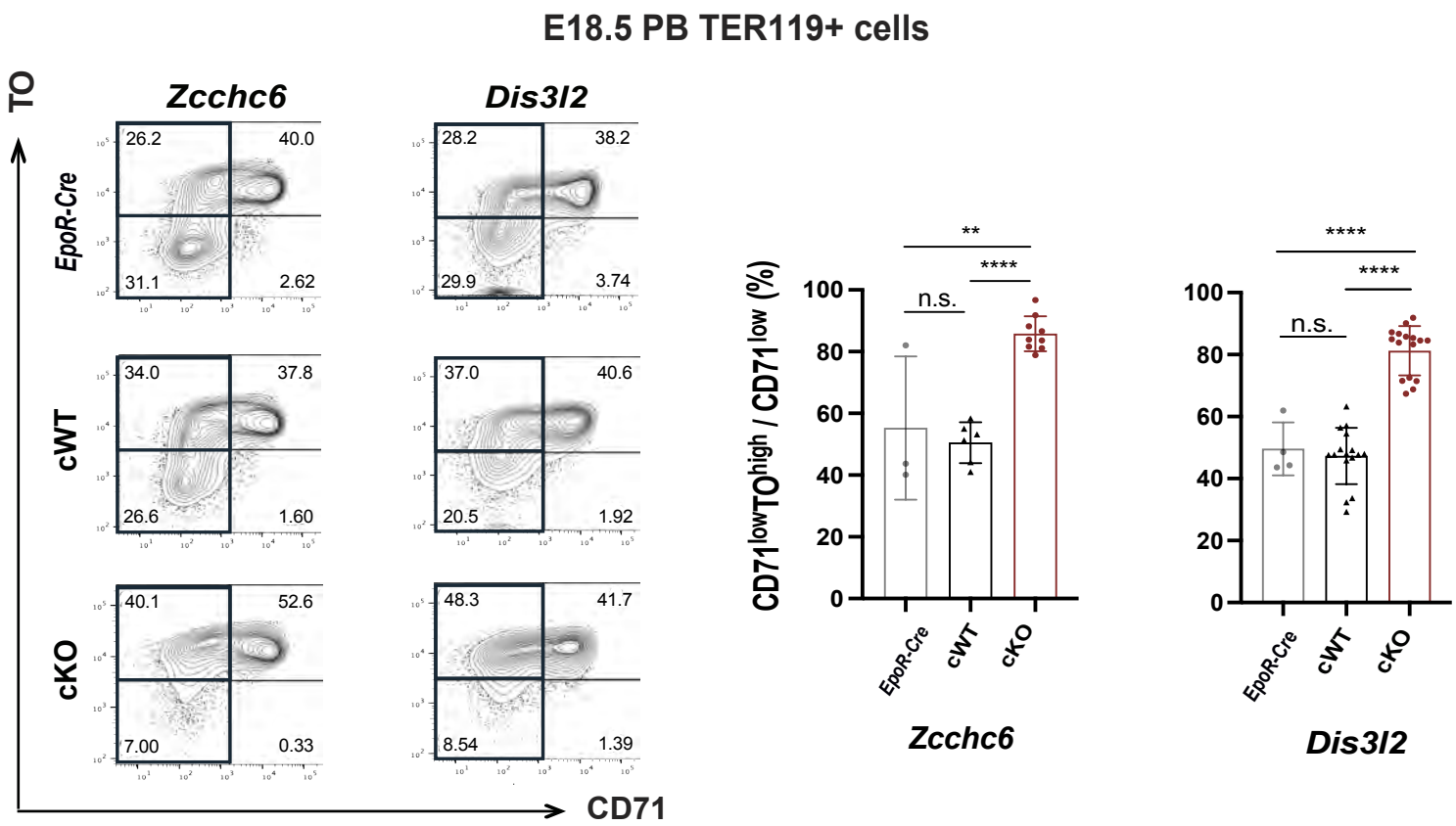

c

p-values (<0.05 *, <0.01 **, <0.001***)

Parameter	Unit	*Zcchc6*			p-value		*Dis3l2*			p-value	
		EpoR-Cre	cWT	cKO	cWT vs. cKO	*EpoR-Cre* vs. cKO	*EpoR-Cre*	cWT	cKO	cWT vs. cKO	*EpoR-Cre* vs. cKO
RBC	M/μl	3.43 ± 0.22	3.45 ± 0.10	3.19 ± 0.14	*	*	3.70 ± 0.56	3.64 ± 0.54	3.49 ± 0.20	*	*
HCT	%	52.00 ± 1.66	51.93 ± 2.03	48.13 ± 4.21			49.00 ± 10.17	48.86 ± 7.66	47.29 ± 4.76		*
MCH	pg	34.28 ± 0.85	34.18 ± 1.98	36.52 ± 1.04	*	*	33.08 ± 2.13	32.71 ± 4.25	33.64 ± 3.09		
MCHC	g/dL	22.58 ± 0.82	22.68 ± 1.31	24.20 ± 0.75			25.13 ± 0.33	24.48 ± 3.68	24.86 ± 2.13		
MCV	fL	151.78 ± 6.82	150.63 ± 4.08	150.85 ± 8.27			131.73 ± 9.68	134.08 ± 8.55	135.50 ± 8.15		
RDW	%	19.38 ± 1.13	18.73 ± 0.43	19.7 ± 0.76			19.58 ± 1.88	19.50 ± 0.79	19.49 ± 1.32		
Hb	g/dL	11.75 ± 0.47	11.78 ± 0.36	11.63 ± 0.77			12.30 ± 2.47	11.74 ± 1.16	11.74 ± 1.42		

Fig. 2. Analysis of Conditional *Zcchc6/Dis3l2* Knockout Mice.
(a) Breeding scheme to generate erythroid-specific, conditional KO mice.
(b, left figures) Representative FACS profiles from peripheral blood of embryos carrying only the *EpoR-Cre* allele (top lane), only the flox allele (cWT, middle lane), and both alleles; erythroid-specific conditional KOs (cKO, bottom lane).
(b, right graphs) Quantification of reticulocyte ($CD71^{low}TO^{high}$) population per genotype.
(c) Hematological profile results from the PB of conditional KOs (erythrocyte panel).

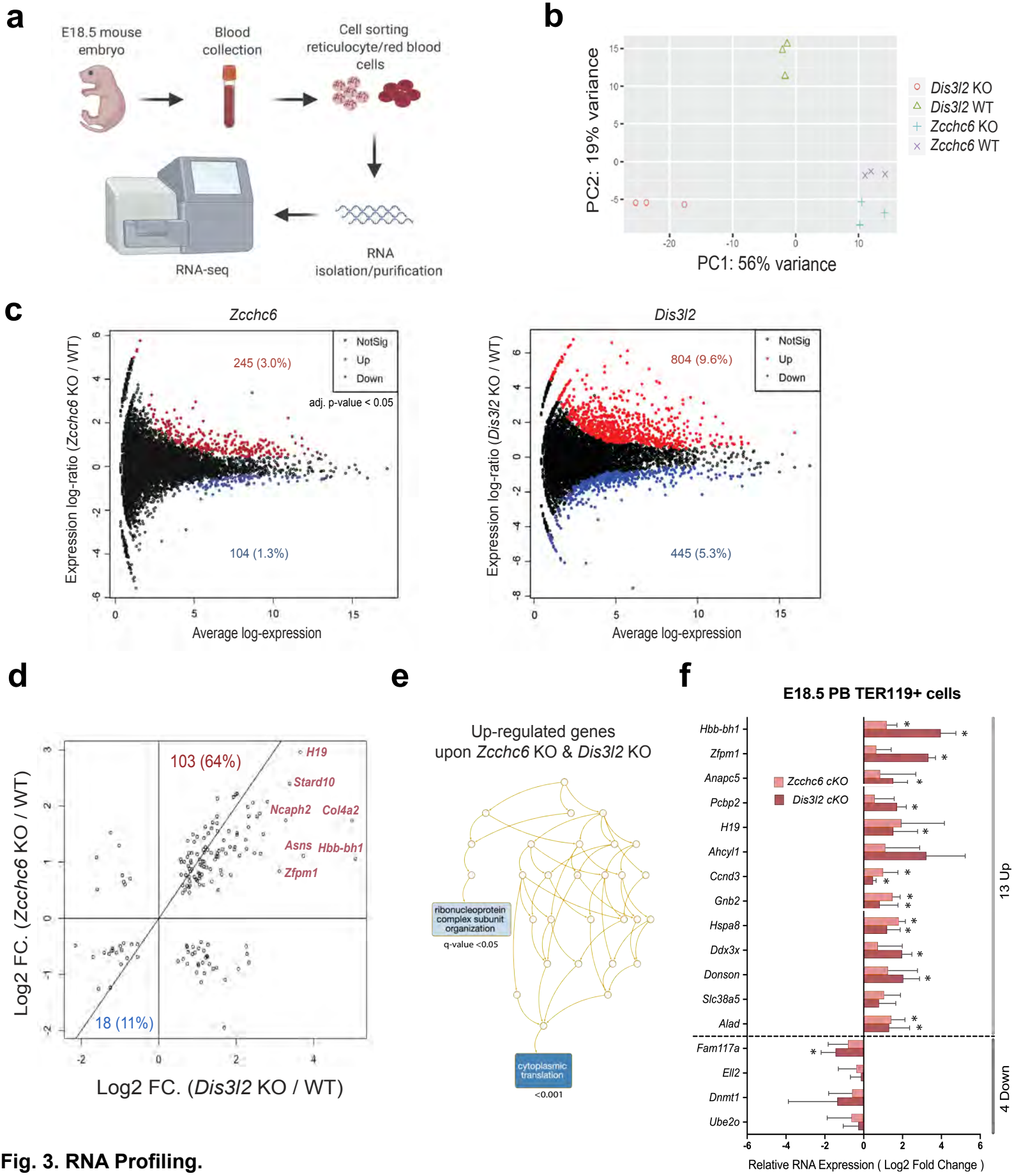

Fig. 3. RNA Profiling.

(a) RNA-seq experimental scheme from embryonic erythroid cells.
(b) Principal component analysis of global transcriptome from *Zcchc6* and *Dis3l2* KOs and corresponding WTs.
(c) Differentially expressed genes in each KO model.
(d) Overlap analysis of differentially expressed genes in each KO model.
(e) Gene ontology analysis of up-regulated genes from both KOs.
(f) Validation of top hits using qPCRs with samples from cKOs.

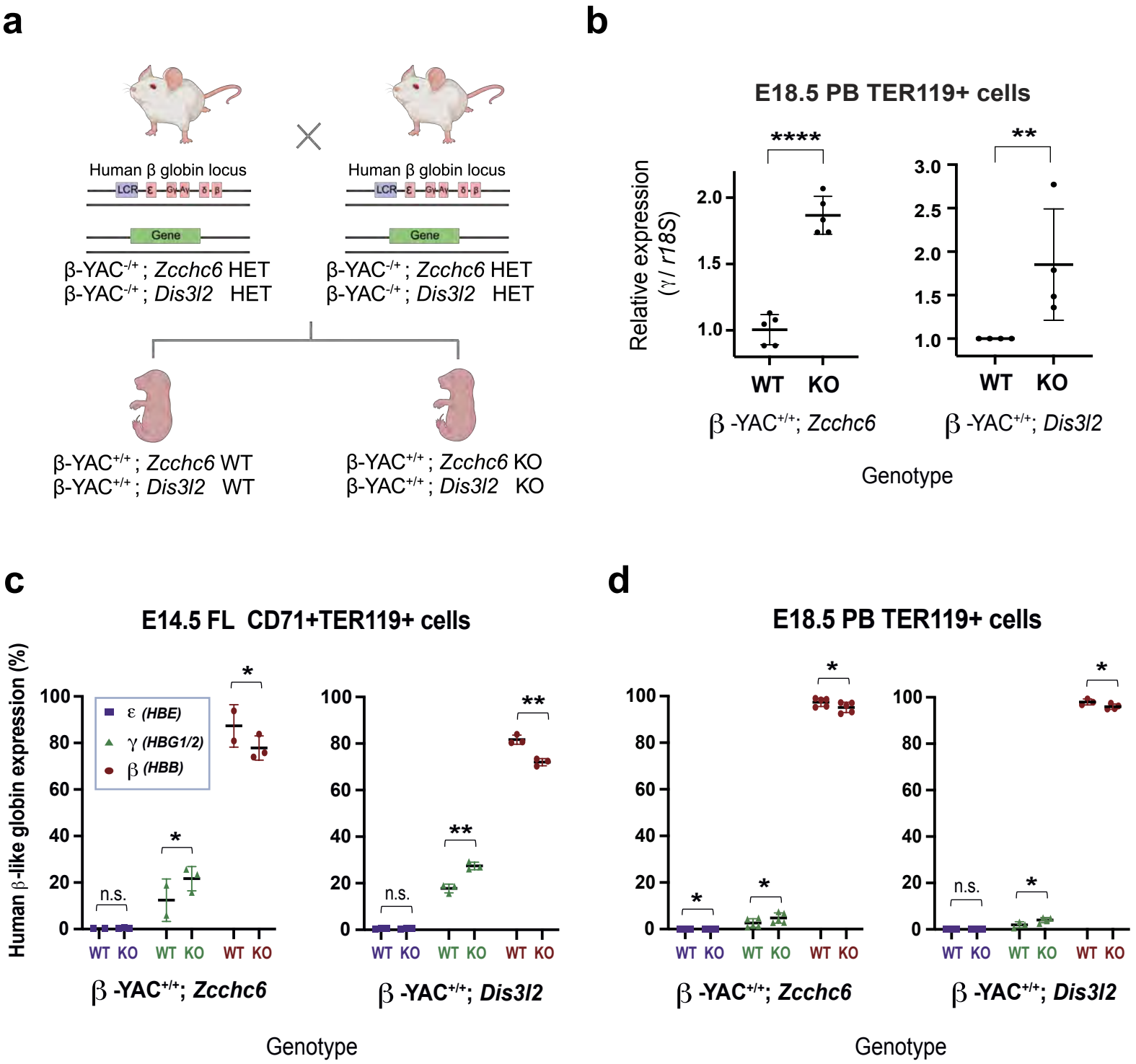

Fig. 4. Humanized Murine Model Study.
(a) Breeding scheme for crossing *Zcchc6/Dis3l2* KO mice with humanized globin YAC mice.
(b) Fold change in normalized *γ-globin* expression (Ct values for *γ-globin* transcripts were first normalized to those of *r18S* transcripts, and the fold change was then calculated relative to the value of littermate WTs).
(c-d) Human *β-like* globin profiles on sorted erythroid cells from E14.5 fetal liver and E18.5 PB of humanized mouse embryos using qPCRs. For each embryonic age and mouse model, embryos from two litters were used.

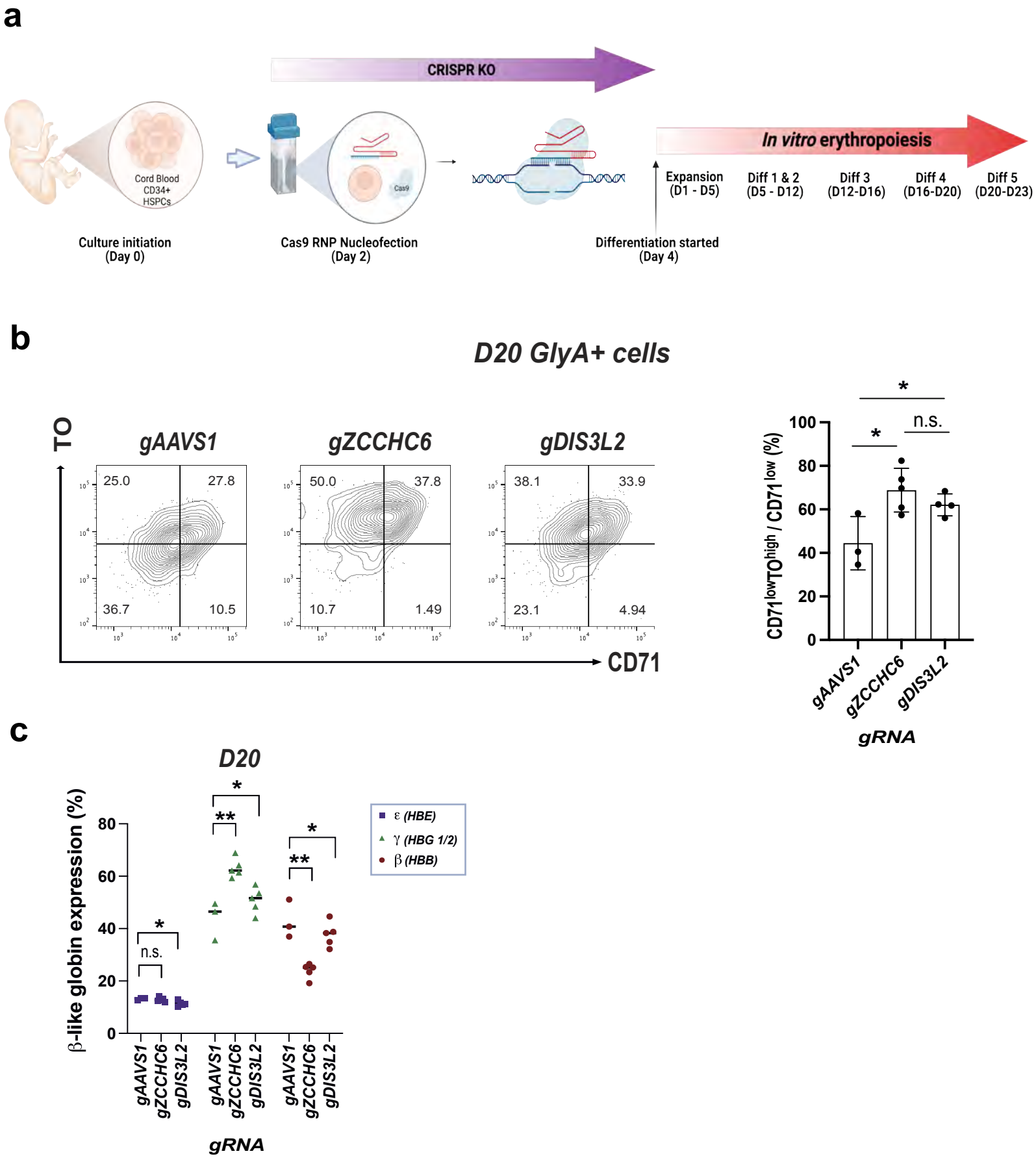

Fig. 5. Human *In Vitro* Erythropoiesis Study Using CRISPR Knockout.
(a) Scheme of the CRISPR/Cas9 knockout followed by *in vitro* erythropoiesis.
(b) Representative profiles of TO and CD71 within erythroid (GlyA+) cells and the corresponding graph with statistical assessment.
(c) Globin profiles upon CRISPR/Cas9 knockouts.

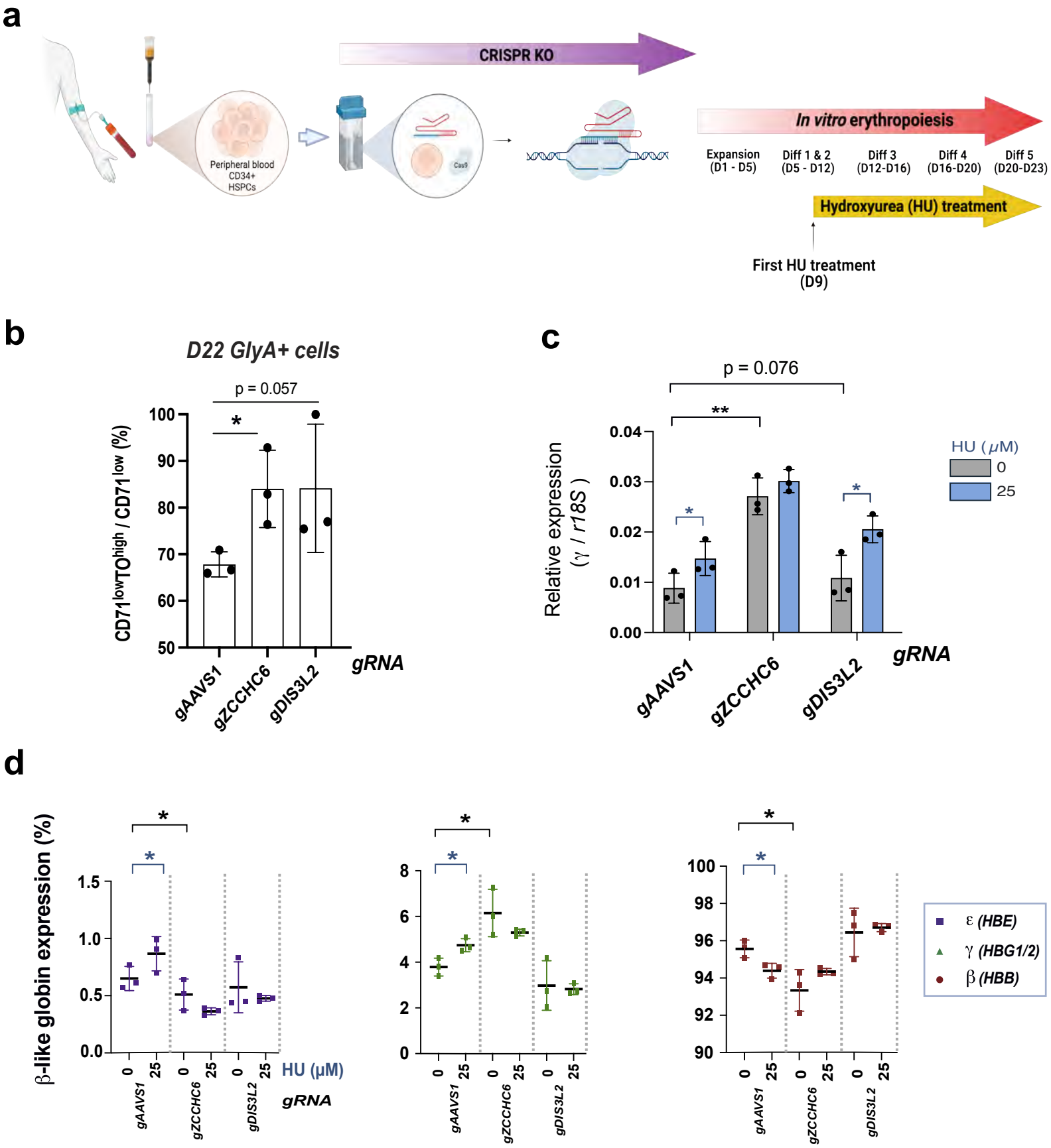

Fig. 6. *In Vitro* Erythropoiesis Study with CRISPR KO and HU(Hydroxyurea) Treatment.
(a) Scheme of the CRISPR/Cas9 knockout and HU treatment followed by *in vitro* erythropoiesis.
(b) Summary graph and statistical assessment of $CD71^{low}TO^{high}$ population upon CRISPR/Cas9 KOs.
(c) Human *γ-globin* mRNA expression upon CRISPR/Cas9 knockouts and HU treatment.
(d) Globin profiles upon CRISPR/Cas9 KOs and HU treatment.

Extended Data Fig. 1

Zcchc6

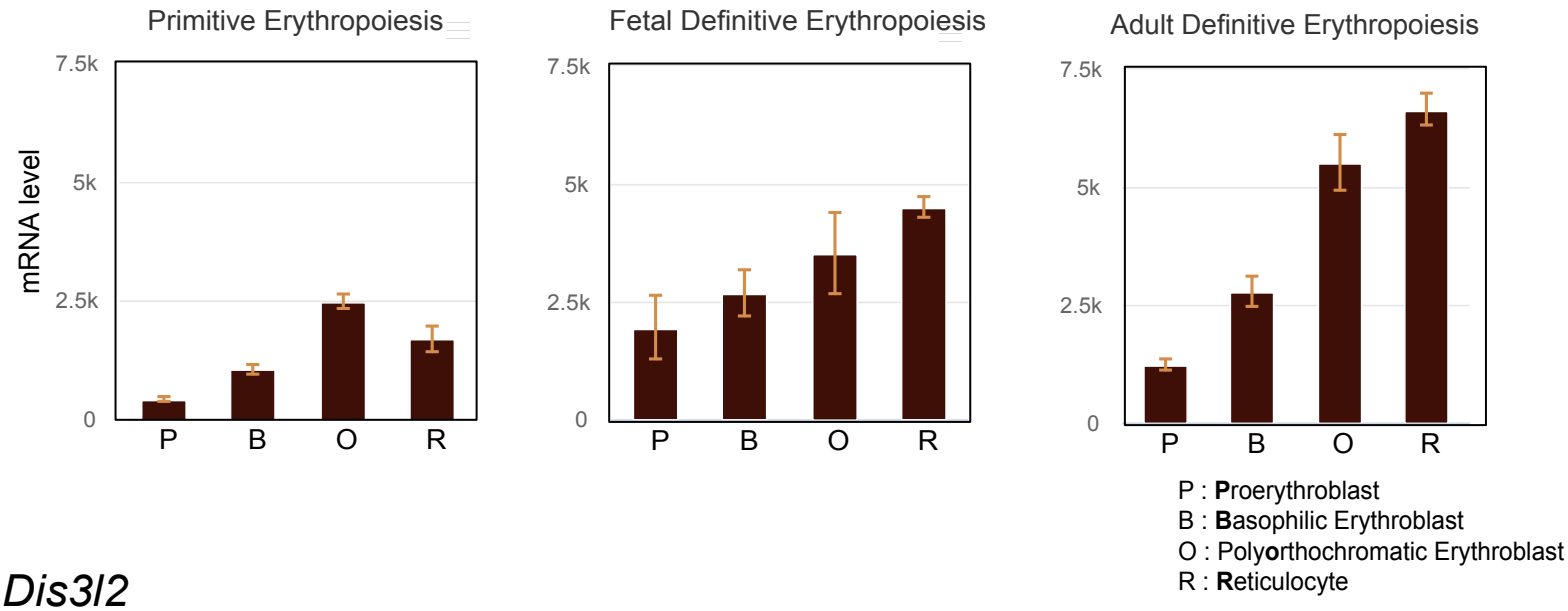

Dis3l2

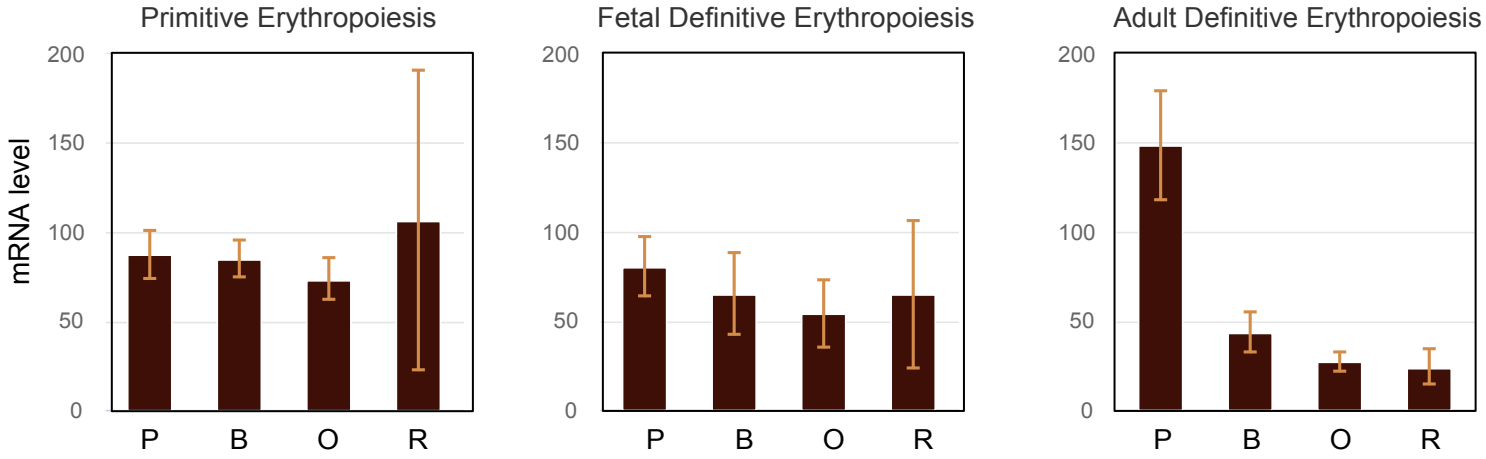

Extended Data Fig. 1.
Expression Profiles of Zcchc6 and Dis3l2 mRNAs During Erythropoiesis (from the Erythron Database).
Expression Levels of Zcchc6 and Dis3l2 mRNAs During Mouse Primitive and Definitive
(fetal liver and adult bone marrow) Erythropoiesis.

Extended Data Fig. 2

a

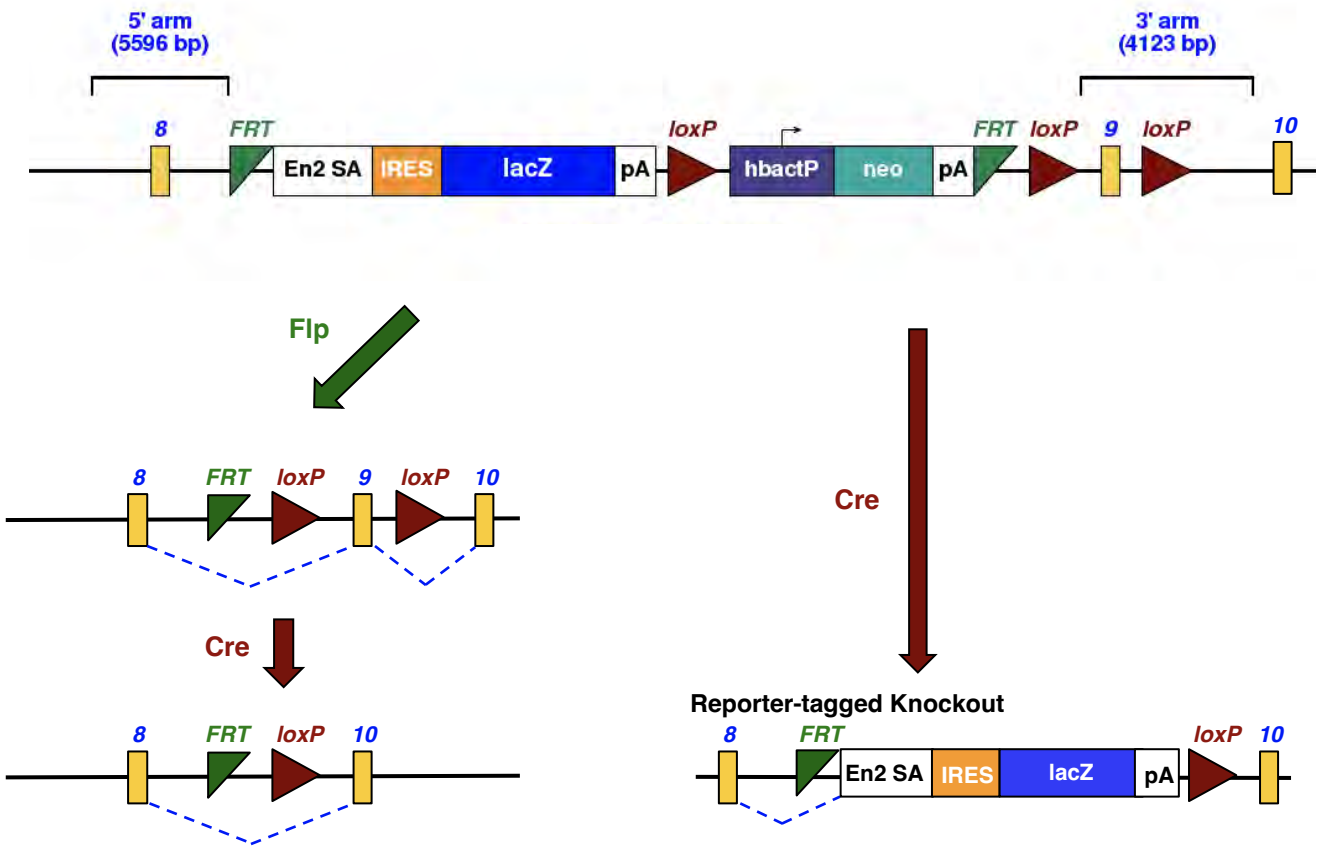

b

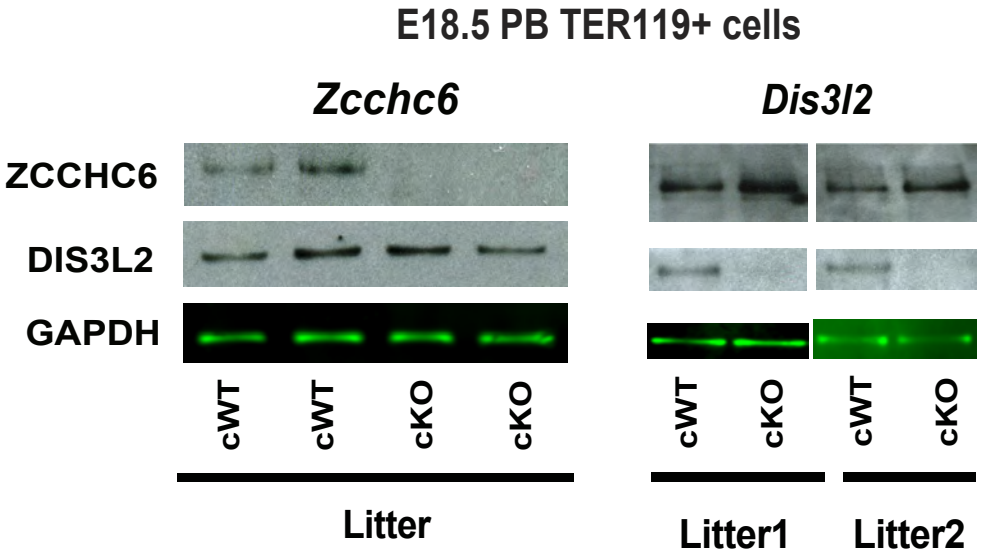

Extended Data Fig. 2. Allele Map of the Dis3l2 Knockout Model and Conditional Knockout Validation.
(a) Allele Map of the *Dis3l2* Knockout Models.
(b) Western Blots of Erythroid Cells from Embryos Carrying only *floxed* (cWT) and both *floxed* and *EpoR-Cre* (cKO) Alleles for Validation.

Extended Data Fig. 3

a

p-values (<0.05 *, <0.01 **, <0.001***)

Parameter	Unit	*Zcchc6*			p-value	
		WT	HET	KO	WT vs. KO	HET vs. KO
RBC	M/µl	9.09 ± 0.39	9.03 ± 0.29	9.05 ± 0.39		
HCT	%	43.28 ± 1.52	43.35 ± 1.71	43.99 ± 1.66		
MCH	pg	14.52 ± 0.73	14.66 ± 0.69	15.15 ± 0.76		
MCHC	g/dL	30.48 ± 0.96	30.55 ± 1.17	31.15 ± 1.24		
MCV	fL	47.65 ± 1.50	48.04 ± 1.44	48.61 ± 1.26		
RDW	%	16.49 ± 0.44	16.74 ± 0.60	16.60 ± 0.47		
Hb	g/dL	13.18 ± 0.57	13.23 ± 0.54	13.70 ± 0.79		

b

p-values (<0.05 *, <0.01 **, <0.001***)

Parameter	Unit	*Zcchc6*			p-value	
		WT	HET	KO	WT vs. KO	HET vs.KO
Leukocytes:						
WBC	K/µl	9.65 ± 1.25	9.56 ± 1.57	10.29 ± 1.41		
LY	K/µl	6.15 ± 0.89	6.17 ± 1.29	6.38 ± 1.04		
NE	K/µl	2.86 ± 0.45	2.67 ± 0.48	3.13 ± 0.52		*
MO	K/µl	0.49 ± 0.20	0.64 ± 0.18	0.67 ± 0.15		
EO	K/µl	0.13 ± 0.08	0.07 ± 0.04	0.09 ± 0.05		
BA	K/µl	0.02 ± 0.01	0.01 ± 0.01	0.01 ± 0.00		
LY	%	63.71 ± 3.99	64.20 ± 5.30	61.88 ± 4.04		
NE	%	29.74 ± 3.29	28.25 ± 4.55	30.54 ± 3.55		*
MO	%	4.96 ± 1.50	6.66 ± 1.50	6.63 ± 1.77		
EO	%	1.40 ± 0.85	0.78 ± 0.50	0.86 ± 0.38		
BA	%	0.19 ± 0.14	0.12 ± 0.10	0.10 ± 0.04		
Thrombocytes:						
PLT	K/µl	870.15 ± 83.11	923.91 ± 120.69	884.38 ± 125.59		
MPV	fL	4.60 ± 0.12	4.63 ± 0.14	4.66 ± 0.15		

c

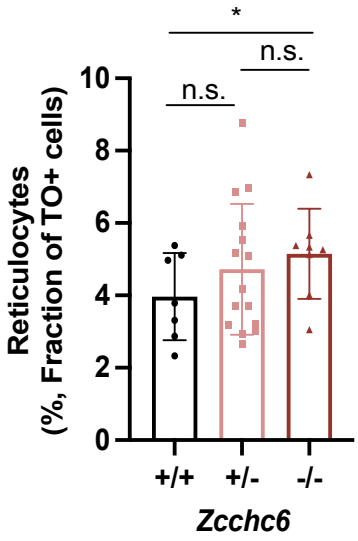

Extended Data Fig. 3. Analysis of Whole-Body *Zcchc6* Knockout Young Adult Mice (6–7 Weeks).

(a) Hematological Profiles of Peripheral Blood from Retro-Orbital Bleeding (mean ± SD).
HCT; Hematocrit, MCH; Mean corpuscular hemoglobin, MCHC; Mean corpuscular hemoglobin concentration, MCV; Mean corpuscular volume, RDW; Red cell Distribution Width. Multiple litters were used.

(b) Leukocytes and Thrombocyte panels.
LY; lymphocytes, NE; neutrophils, MO; monocytes, EO; eosinophils, BA; basophils,
PLT; Platelet or thrombocyte count, MPV; Mean Platelet Volume.

(c) Quantification of reticulocyte (TO+) population per genotype (mean ± SD).

Extended Data Fig. 4

a

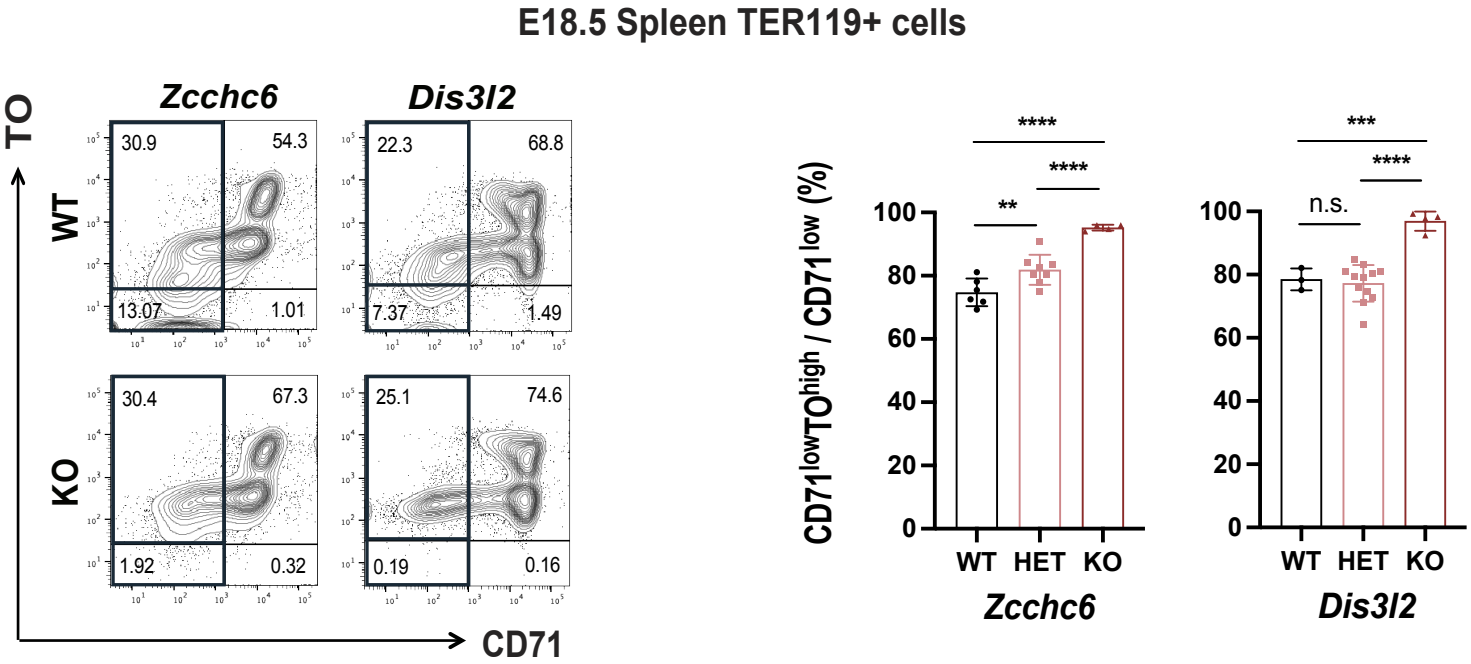

b

p-values (<0.05 *, <0.01 **, <0.001***)

Parameter	Unit	*Zcchc6*			p-value		*Dis3l2*			p-value	
		WT	HET	KO	WT vs. KO	HET vs.KO	WT	HET	KO	WT vs. KO	HET vs. KO
Leukocytes:											
WBC	K/μl	7.10 ± 1.39	8.96 ± 3.72	21.13 ± 8.52	***	***	3.79 ± 1.22	4.42 ± 1.08	5.53 ± 1.36	*	
LY	K/μl	5.85 ± 1.25	7.60 ± 3.50	18.61 ± 7.52	***	***	1.65 ± 0.62	1.96 ± 0.49	2.77 ± 1.10	*	*
NE	K/μl	0.96 ± 0.14	0.98 ± 0.31	1.66 ± 0.74	**	**	1.58 ± 0.57	1.82 ± 0.57	2.00 ± 0.73		
MO	K/μl	0.17 ± 0.08	0.22 ± 0.07	0.71 ± 0.29	***	***	0.12 ± 0.10	0.12 ± 0.09	0.15 ± 0.09		
EO	K/μl	0.10 ± 0.04	0.11 ± 0.05	0.12 ± 0.04			0.34 ± 0.11	0.43 ± 0.18	0.46 ± 0.10		
BA	K/μl	0.04 ± 0.01	0.04 ± 0.02	0.05 ± 0.03			0.10 ± 0.05	0.10 ± 0.05	0.16 ± 0.09		*
LY	%	82.10 ± 2.33	83.63 ± 5.61	87.87 ± 1.61			43.52 ± 9.67	44.52 ± 7.34	49.51 ± 11.79		
NE	%	13.75 ± 2.22	11.93 ± 4.92	7.92 ± 1.44	*		41.88 ± 9.86	40.86 ± 6.63	36.35 ± 9.34		
MO	%	2.24 ± 0.92	2.60 ± 0.63	3.38 ± 0.63	*		2.73 ± 1.84	2.75 ± 2.05	2.51 ± 1.23		
EO	%	1.37 ± 0.44	1.37 ± 0.61	0.60 ± 0.21		*	9.37 ± 1.14	9.64 ± 3.13	8.58 ± 2.26		
BA	%	0.54 ± 0.06	0.47 ± 0.19	0.22 ± 0.09	**	**	2.51 ± 1.15	2.23 ± 1.16	3.05 ± 1.26		
Thrombocytes:											
PLT	K/μl	496.75 ± 49.31	517.67 ± 35.27	519.13 ± 24.93			425.60 ± 71.20	464.71 ± 86.20	411.64 ± 66.27		
MPV	fL	6.31 ± 0.17	6.42 ± 0.15	6.50 ± 0.11			6.32 ± 0.18	6.10 ± 0.27	6.13 ± 0.22		

Extended Data Fig. 4. Additional Analysis of Whole-Body *Zcchc6/Dis3l2* Knockout Mice.
(a, left figures) Flow cytometry profiles of erythroid cells from spleens.
Representative profiles of each KO mouse and WT littermates were displayed.
(a, right graphs) Quantification of reticulocyte population per genotype.
(b) Hematological profiles in the PB of whole-body KOs (Leukocytes and Thrombocyte panels).
LY; lymphocytes, NE; neutrophils, MO; monocytes, EO; eosinophils, BA; basophils,
PLT; Platelet or thrombocyte count, MPV; Mean Platelet Volume.

Extended Data Fig. 5

a

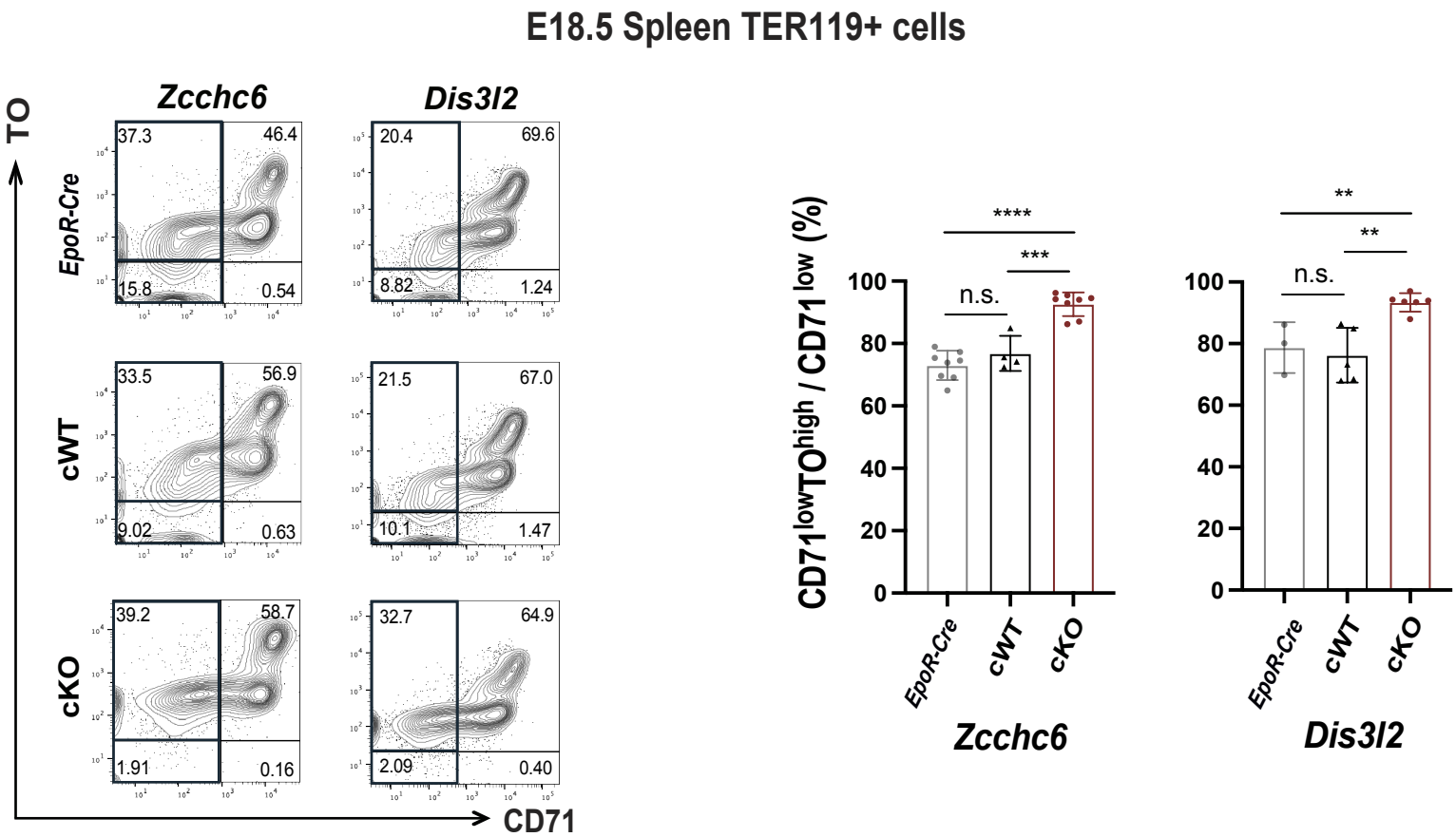

b

p-values (<0.05 *, <0.01 **, <0.001***)

Parameter	Unit	*Zcchc6*			p-value		*Dis3l2*			p-value	
		EpoR-Cre	cWT	cKO	cWT vs. cKO	*EpoR-Cre* vs. cKO	*EpoR-Cre*	cWT	cKO	cWT vs. cKO	*EpoR-Cre* vs. cKO
Leukocytes:											
WBC	K/µl	15.60 ± 5.12	16.54 ± 6.04	30.89 ± 11.89	0.0686	*	17.14 ± 15.10	13.37 ± 7.68	26.49 ± 16.83	***	*
LY	K/µl	14.28 ± 5.13	15.24 ± 5.72	27.93 ± 11.59	0.0913	*	15.49 ± 14.10	12.25 ± 7.40	24.19 ± 15.79	***	*
NE	K/µl	0.92 ± 0.21	0.86 ± 0.20	1.86 ± 0.89			1.18 ± 0.49	0.88 ± 0.25	1.49 ± 0.52	**	
MO	K/µl	0.32 ± 0.13	0.36 ± 0.22	0.91 ± 0.43		*	0.40 ± 0.55	0.17 ± 0.17	0.73 ± 0.66	**	
EO	K/µl	0.06 ± 0.03	0.06 ± 0.03	0.16 ± 0.08			0.06 ± 0.04	0.06 ± 0.03	0.04 ± 0.02		
BA	K/µl	0.03 ± 0.01	0.02 ± 0.01	0.03 ± 0.01			0.02 ± 0.01	0.02 ± 0.01	0.02 ± 0.01		
LY	%	90.50 ± 4.55	91.88 ± 1.40	89.39 ± 4.33			87.57 ± 7.37	88.59 ± 7.74	90.05 ± 3.11		
NE	%	6.85 ± 4.25	5.58 ± 1.66	7.21± 4.31			10.20 ± 7.96	9.72 ± 7.94	7.41 ± 3.66	*	
MO	%	1.99 ± 0.27	2.02 ± 0.70	2.77 ± 1.08			1.74 ± 0.93	0.94 ± 0.64	2.21 ± 1.09	***	
EO	%	0.47 ± 0.38	0.36 ± 0.20	0.51 ± 0.13			0.38 ± 0.18	0.56 ± 0.34	0.21 ± 0.10	*	
BA	%	0.20 ± 0.15	0.17 ± 0.11	0.11 ± 0.08			0.12 ± 0.06	0.17 ± 0.11	0.11 ± 0.11		
Thrombocytes:											
PLT	K/µl	590.75 ± 38.23	579.50 ± 16.09	609.67 ± 48.13			610.5 ± 133.57	609.11 ± 94.52	569.50 ± 57.43		
MPV	fL	6.00 ± 0.14	6.10 ± 0.18	6.02 ± 0.13			5.98 ± 0.15	6.12 ± 0.16	6.06 ± 0.28		

Extended Data Fig. 5. Additional Analysis of Conditional *Zcchc6/Dis3l2* KO.
(a) Flow cytometry profiles of erythroid cells from the spleen.
Representative profiles and reticulocyte quantification of embryos carrying only the *EpoR-Cre* allele, only the *floxed* allele; cWTs, and both alleles; cKOs.
(b) Hematological profiles in the PB of conditional KOs. (Leukocytes and Thrombocyte panels).
LY; lymphocytes, NE; neutrophils, MO; monocytes, EO; eosinophils, BA; basophils, PLT; Platelet or thrombocyte count, MPV; Mean Platelet Volume.

Extended Data Fig. 6

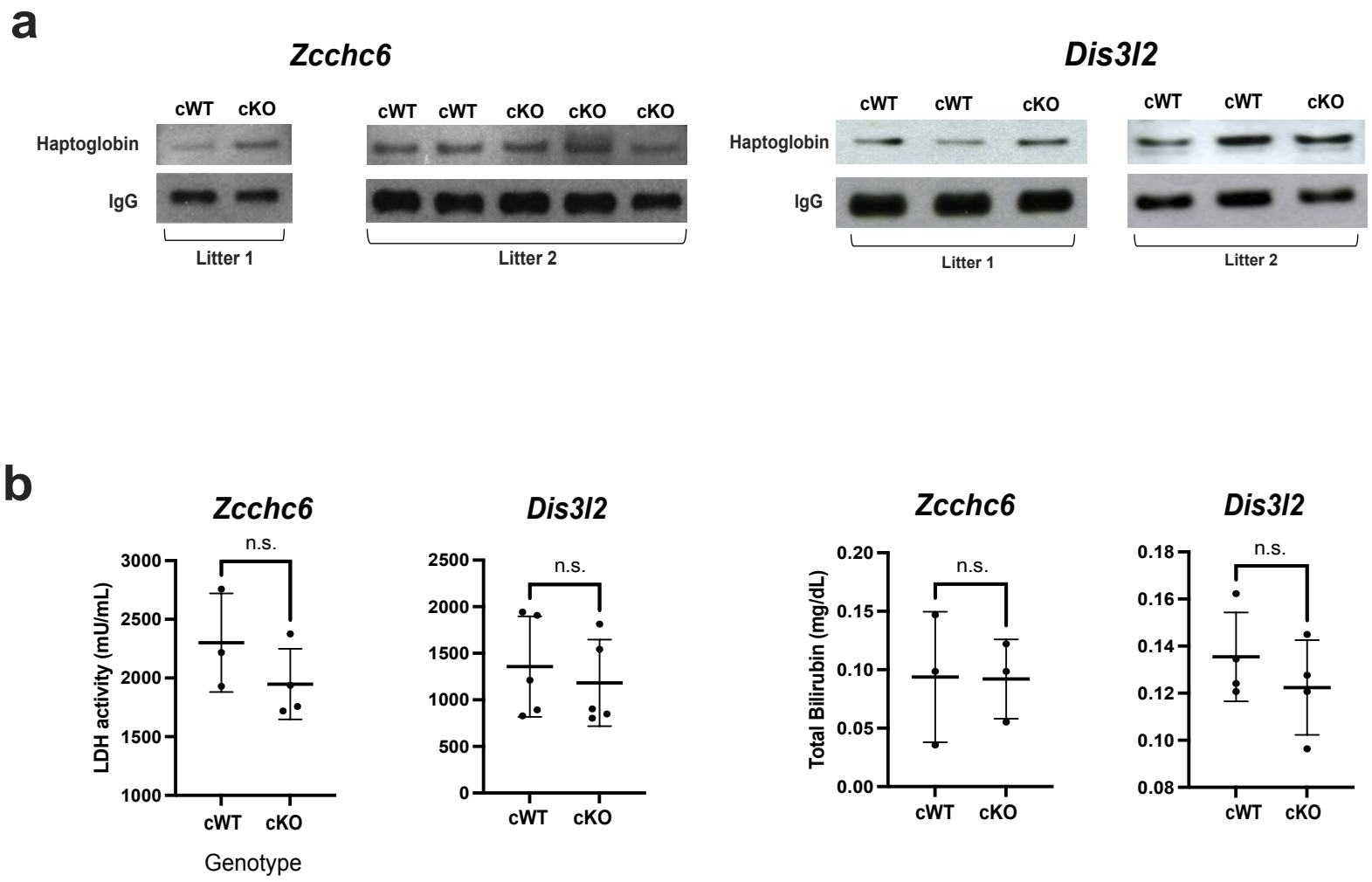

Extended Data Fig. 6. Analysis of Hemolytic Anemia Markers.
(a) Western blots of Haptoglobin in cKOs and cWTs.
(b) LDH and Bilirubin assay results from serum and plasma of cKO mice.

Extended Data Fig. 7

a

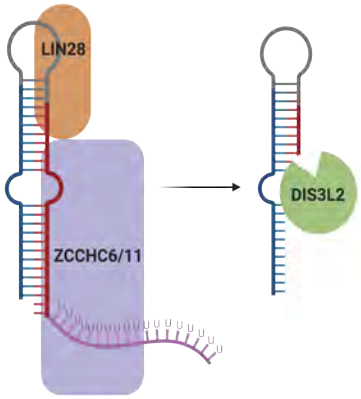

b

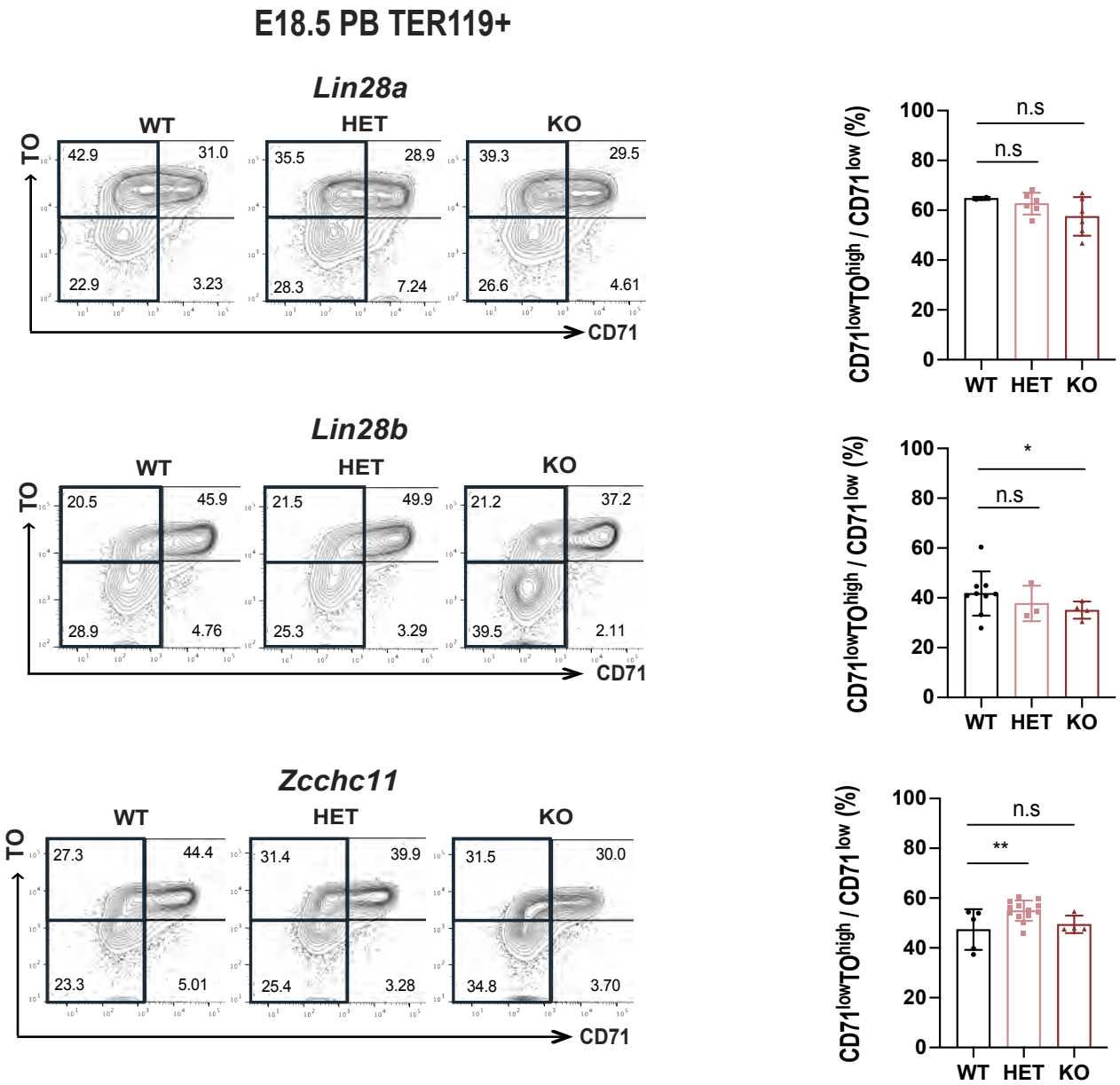

Extended Data Fig. 7. Characterizing the Impact of Knockouts in Pathway-Related Genes.
(a) Previously published model for the RNA decay machinery (LIN28-ZCCHC6/11-DIS3L2) on the microRNA regulation.
(b) FACS profiles and population quantification for each whole-body KO model (*Lin28a*, *Lin28b*, and *Zcchc11* sequentially).

Extended Data Fig. 8

a

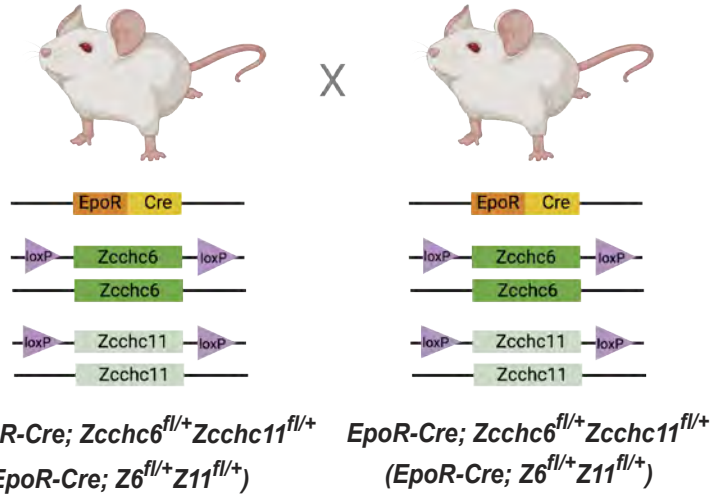

b

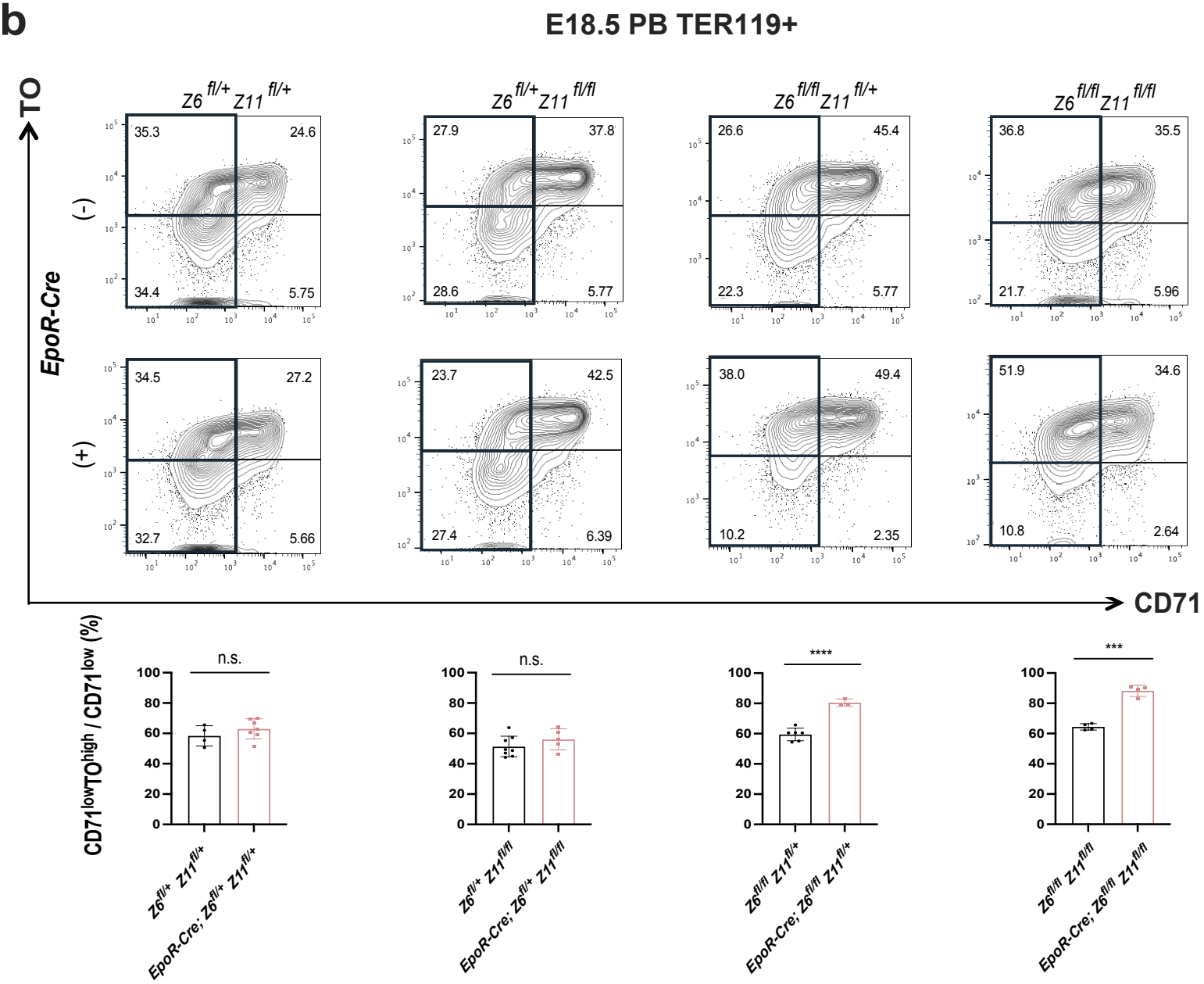

Extended Data Fig. 8. Analysis of *Quad-floxed* Conditional Knockouts.
(a) *Quad-floxed* conditional KO breeding scheme for *Zcchc6* and its paralog *Zcchc11*.
(b) Representative FACS profiles of the *quad-floxed* embryos and quantification of reticulocytes.

Extended Data Fig. 9

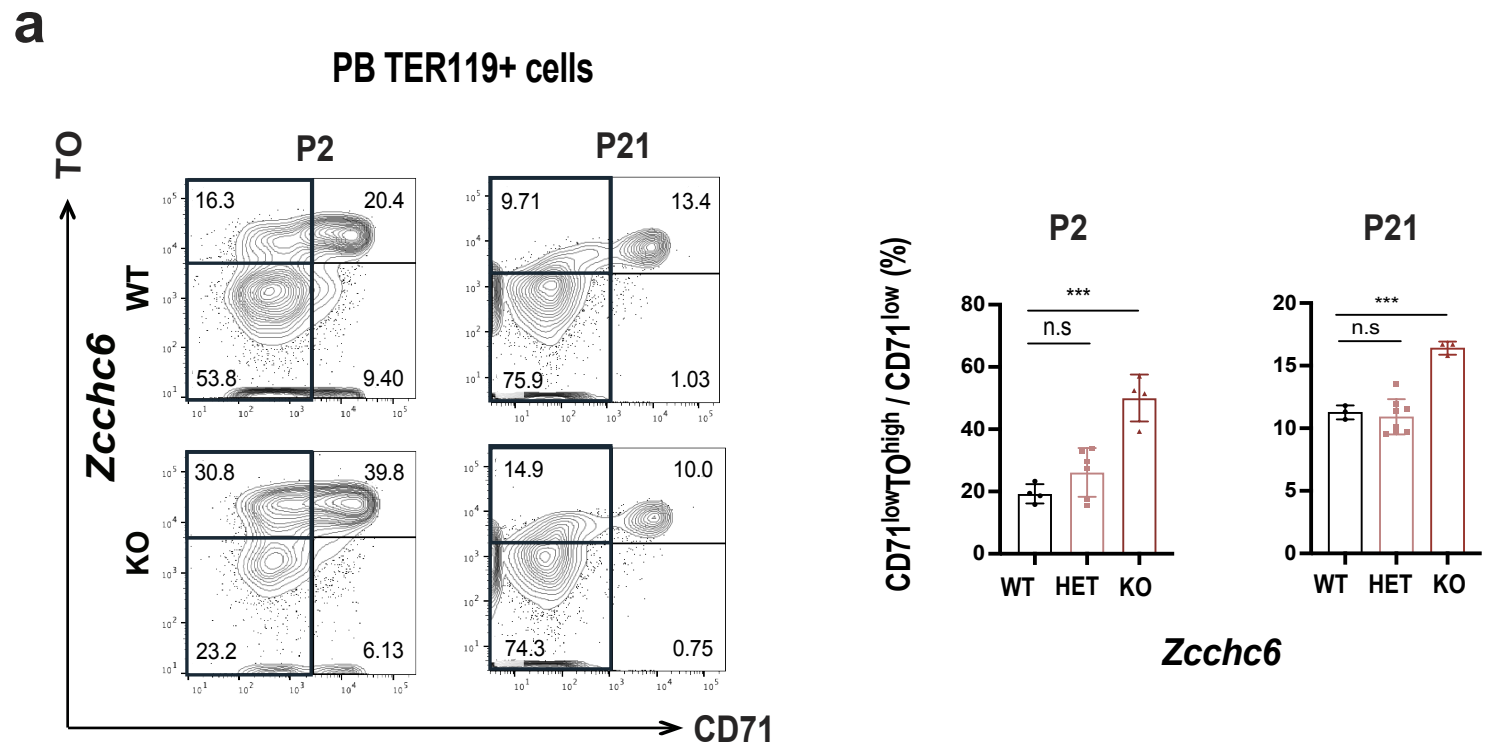

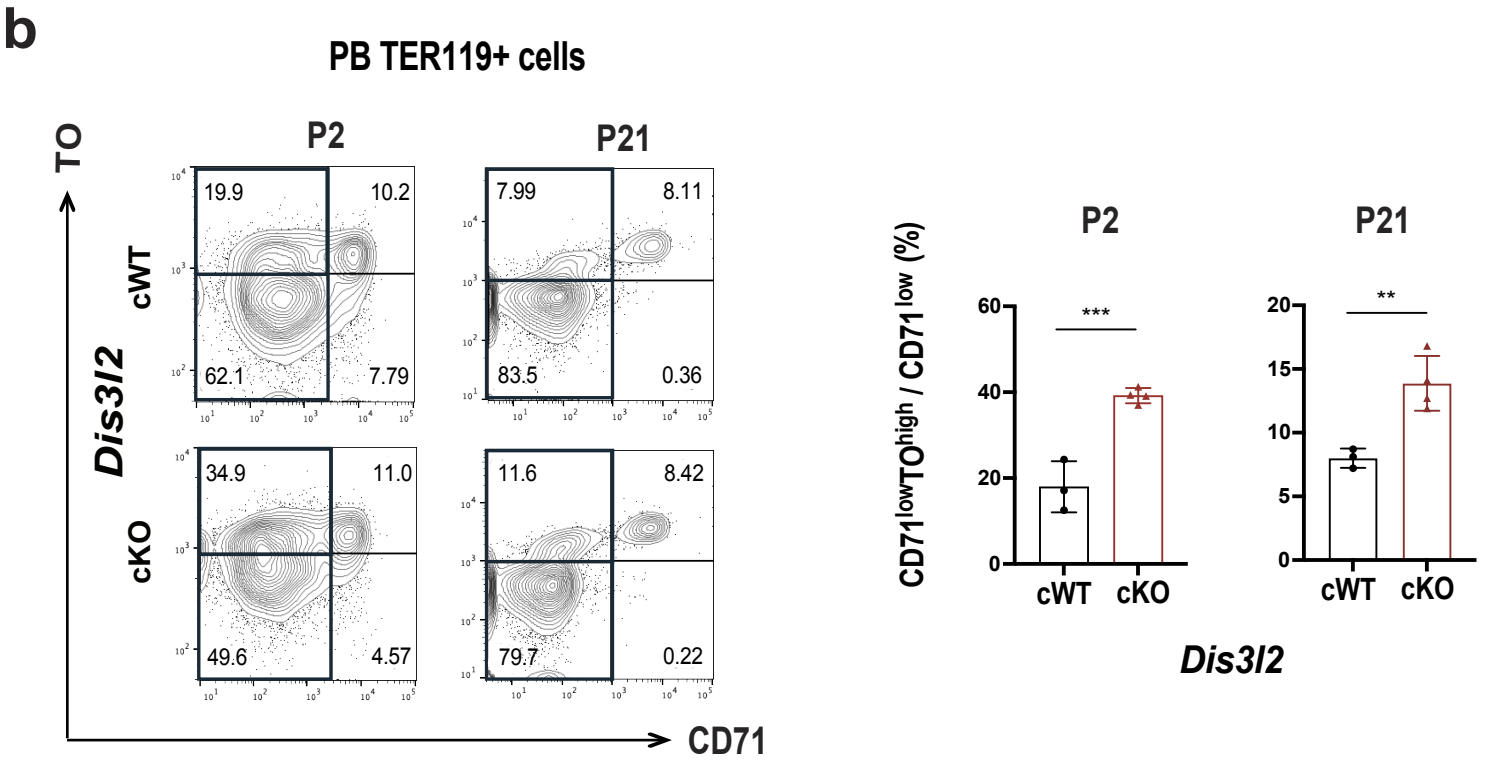

Extended Data Fig. 9. Postnatal Profiling of *Zcchc6* KO and *Dis3l2* cKO.
(a) Postnatal PB FACS profiling and quantification of whole body *Zcchc6* KO model
(b) and *Dis3l2* cKO model.

Extended Data Fig. 10

a

Genotype	Litter	Total Read No.	Mapped Read No.	Mapping Rate
Zcchc6 WT	L3	78,543,026	36,284,397	46.2%
Zcchc6 WT	L4	90,445,954	51,073,608	56.5%
Zcchc6 WT	L5	59,412,646	30,752,512	51.8%
Zcchc6 KO	L3	81,304,604	37,445,722	46.1%
Zcchc6 KO	L4	79,495,636	44,989,077	56.6%
Zcchc6 KO	L5	74,278,610	37,835,979	50.9%
Dis3l2 WT	L1	68,767,710	36,391,345	52.9%
Dis3l2 WT	L2	72,958,170	35,684,609	48.9%
Dis3l2 WT	L2	64,899,346	32,206,562	49.6%
Dis3l2 KO	L1	76,216,868	36,395,571	47.8%
Dis3l2 KO	L2	70,791,404	27,438,581	38.8%
Dis3l2 KO	L2	75,760,250	35,673,350	47.1%

b

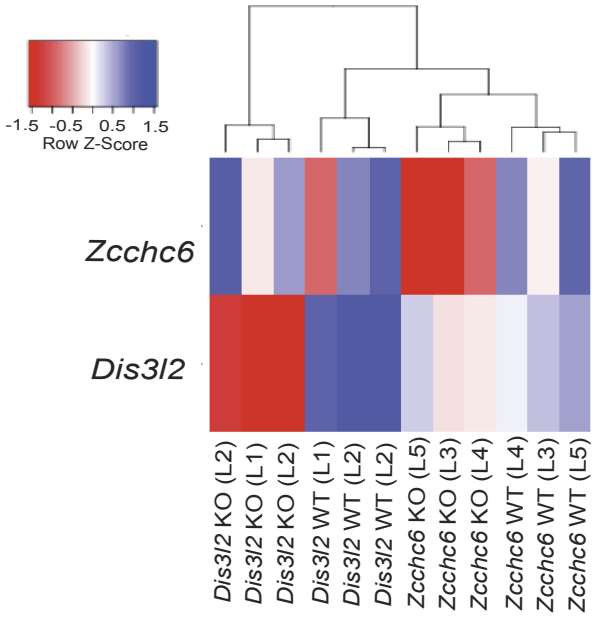

c

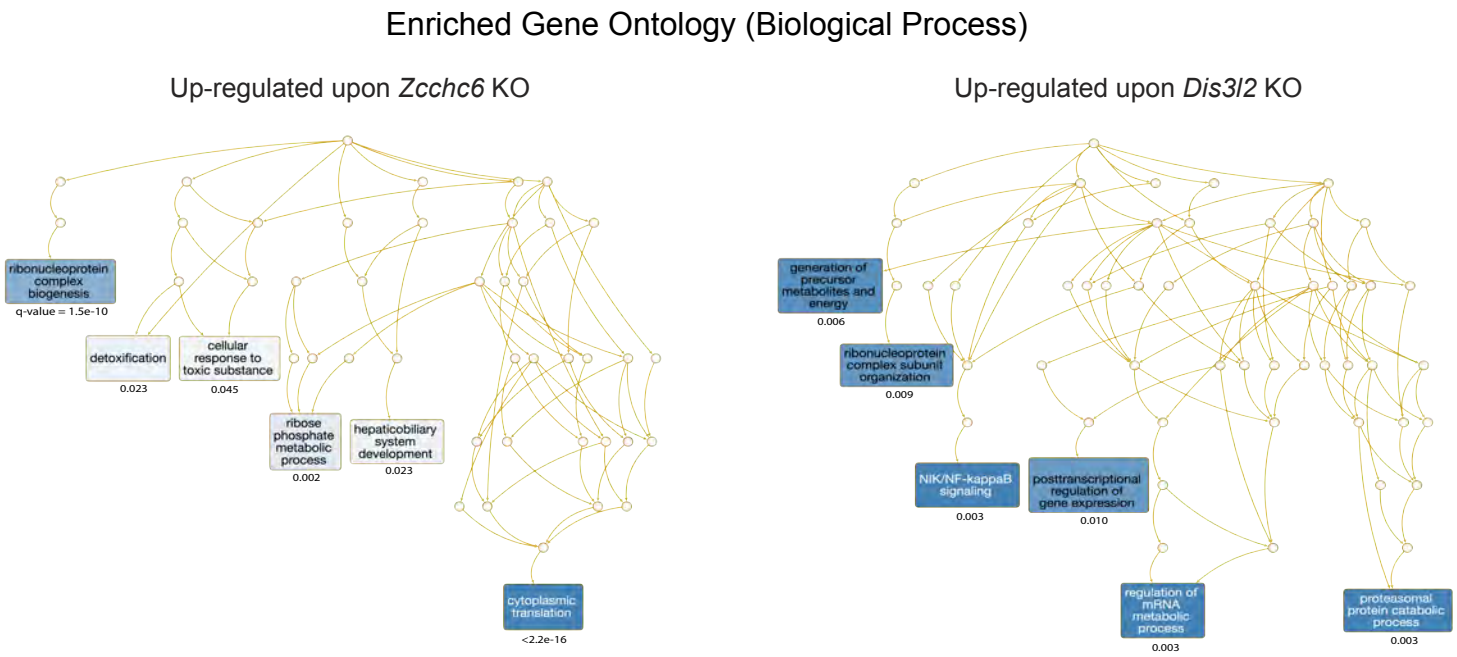

Extended Data Fig. 10. RNA-seq Data Analysis.
(a) Depth and mapping rates of bulk RNA-seq experiments.
(b) Hierarchical clustering of samples based on the expression of *Zcchc6* and *Dis3l2*.
(c) Enriched gene ontology terms and their statistical significances for each KO model.

Extended Data Fig. 11

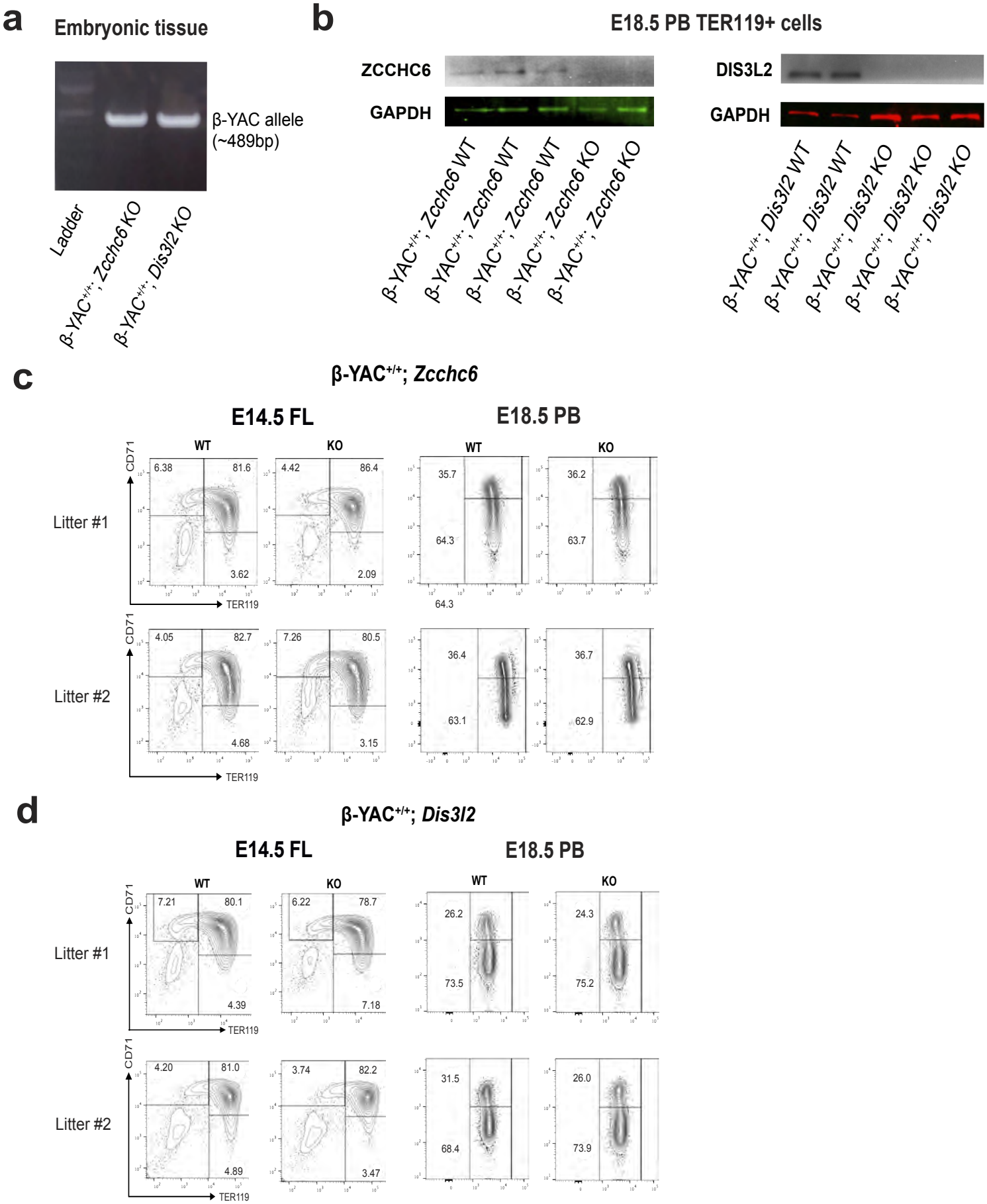

Extended Data Fig. 11. Analysis of Humanized Mice Upon *Zcchc6/Dis3l2* KO.
(a) Genomic PCR analysis of the human β-YAC allele in offspring.
(b) Validation of preserved *Zcchc6/Dis3l2* KO in the crossed humanized mice using western blots.
(c & d) FACS profiles of erythroid maturation from E14.5 fetal liver and E18.5 PB of subject mice.

Extended Data Fig. 12

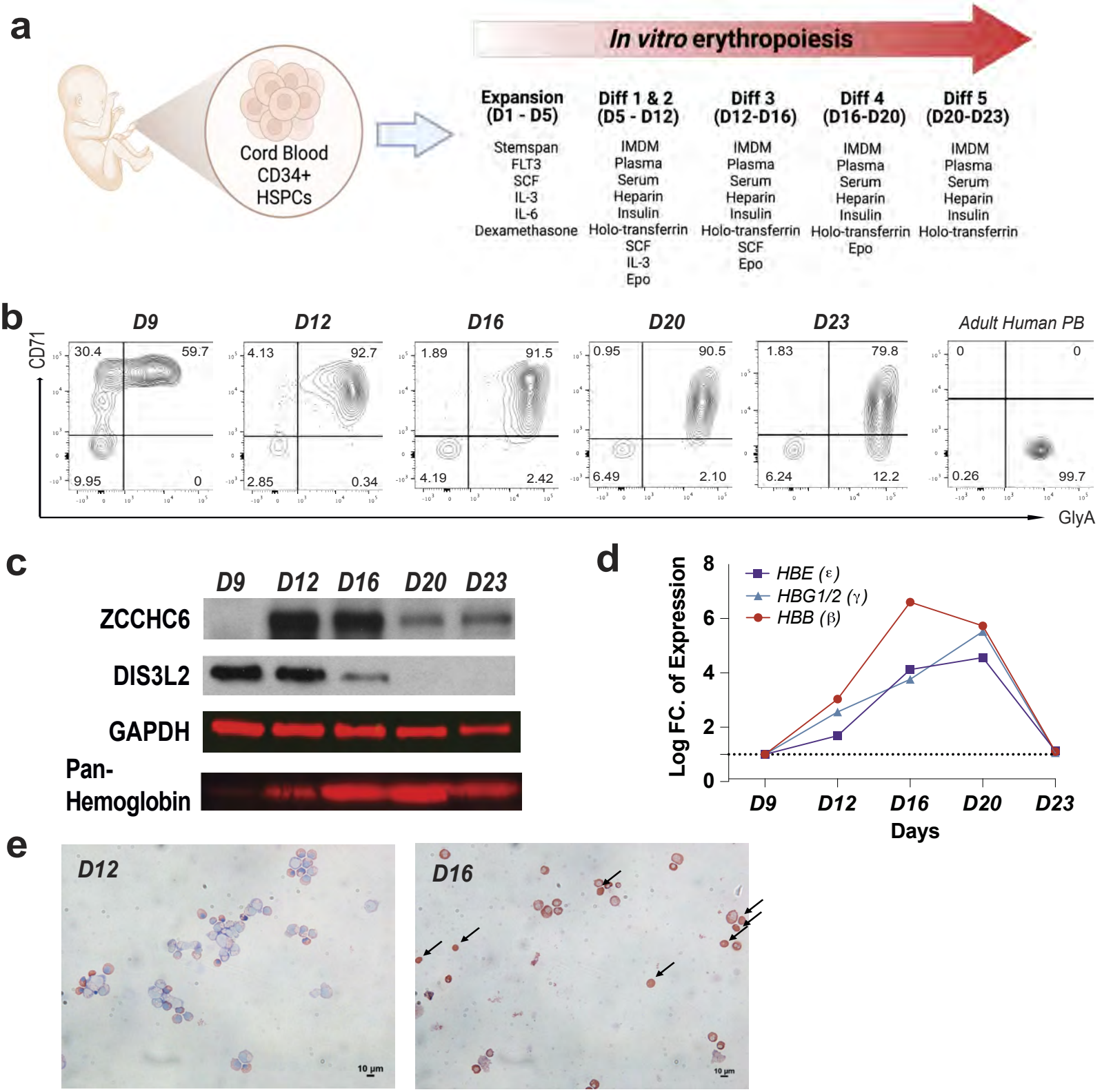

Extended Data Fig. 12. Human *In Vitro* Erythropoiesis

(a) Scheme of *in vitro* erythropoiesis from human cord blood-derived hematopoietic stem/progenitor cells (HSPCs; CD34+ cells).

(b) Time-series FACS profiles to follow erythroid maturation status (Adult human PB served as a positive control).

(c) Time-series protein expression profiles of ZCCHC6, DIS3L2, and hemoglobin during the *in vitro* erythropoiesis by western blots.

(d) RNA expression profiles of β-like globins using qPCRs during the in vitro erythropoiesis.

(e) Histology of cytospined cells (stained by May-Grünwald Giemsa method).

Extended Data Fig. 13

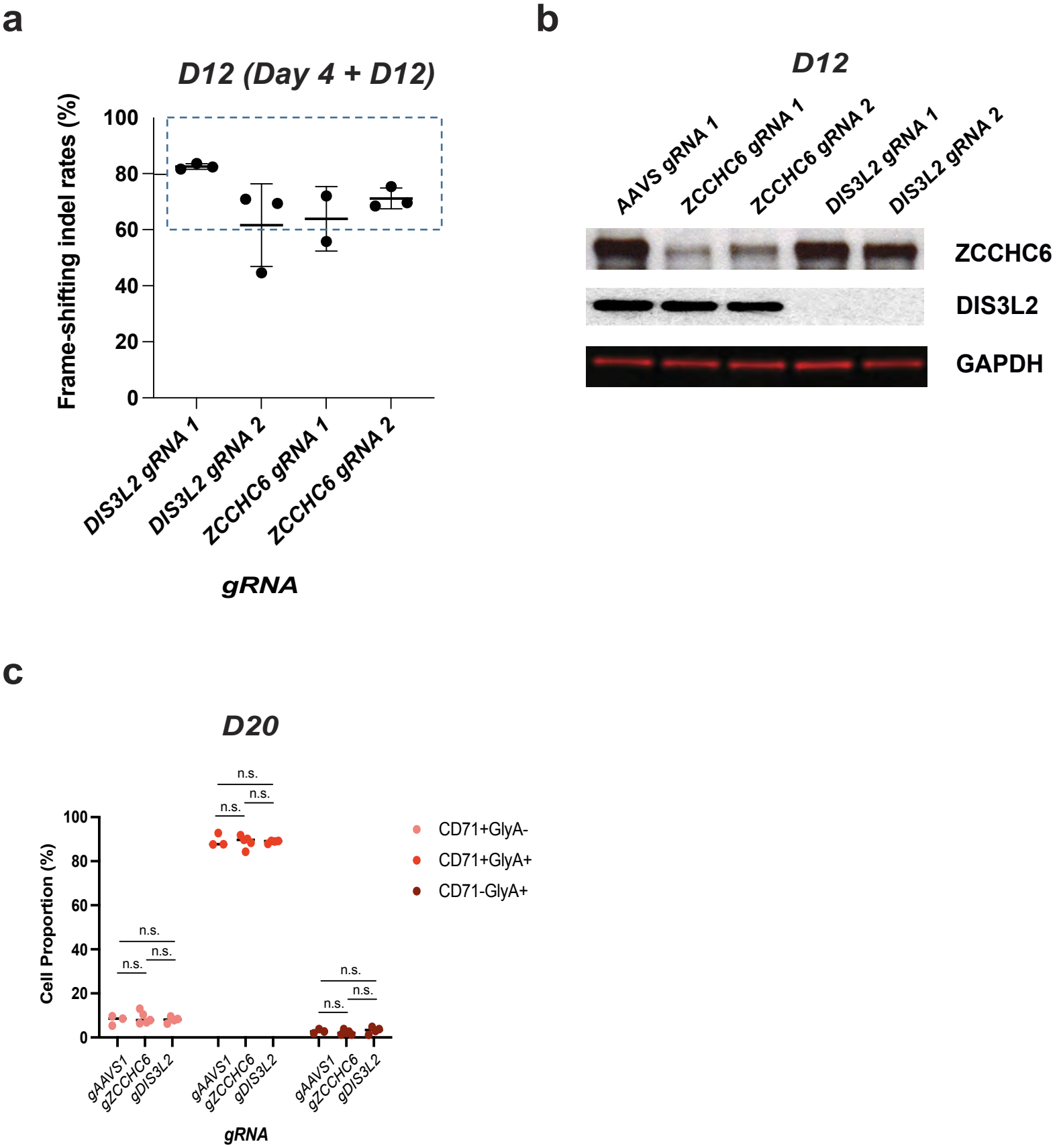

Extended Data Fig. 13. Analysis of CRISPR KO in Differentiated Erythroid Cells from CB.
(a) Genomic editing and **(b)** Protein profiles to access efficiency of CRISPR/Cas9-mediated KOs.
(c) Summary graph of erythroid maturation status by FACS (CD71 and GlyA) in CRISPR/Cas9 KOs.

Extended Data Fig. 14

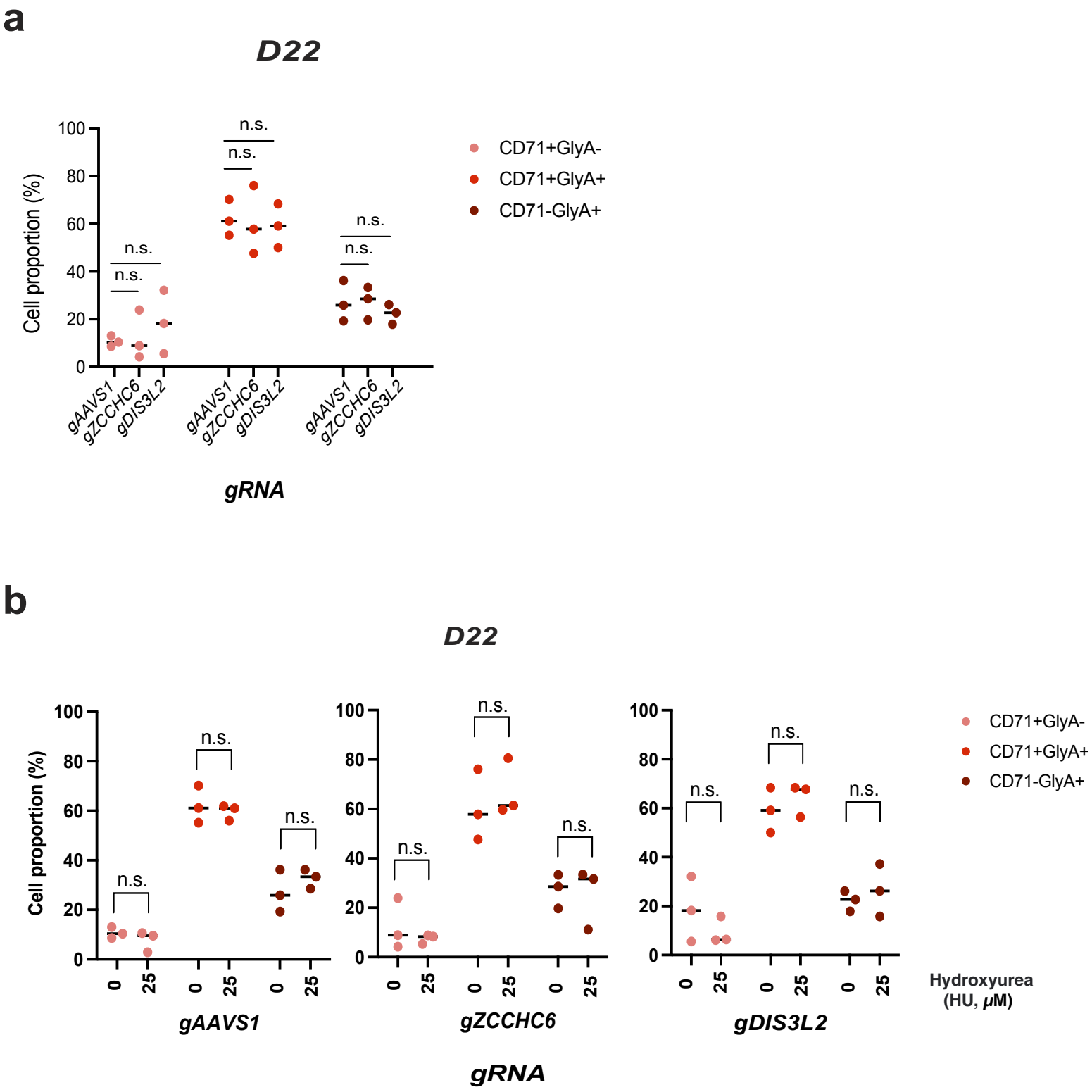

Extended Data Fig. 14.
Analysis of CRISPR KO in Differentiated Erythroid Cells from PB Following HU treatment.
Summary graph of erythroid maturation status by FACS (CD71 and GlyA) in **(a)** CRISPR/Cas9 KOs **(b)** CRISPR/Cas9 KOs & HU treatment

SUPPLEMENTAL TABLES

Supplemental Table 1

qPCR Primers for RNA-seq Validation

Category	Gene	Source	Forward primer seq	Reverse primer seq	Reference
Up	*Hbb-bh1*	Literature			McGrath *et al.* (PubMed ID:21378272)
Up	*Zfpm1*	Commercial			OriGene;MP219016
Up	*Anapc5*	Commercial			OriGene;MP200648
Up	*Pcbp2*	Commercial			OriGene;MP221925
Up	*H19*	Literature	AAGAGCTCGGACTGGAGACT	GACCACACCTGTCATCCTCG	Giovarelli *et al.* (PubMed ID:25385579)
Up	*Ahcyl1*	Commercial			OriGene;MP214966
Up	*Ccnd3*	Commercial			OriGene;MP221497
Up	*Gnb2*	Commercial			OriGene;MP205834
Up	*Hspa8*	Commercial			OriGene;MP205962
Up	*Ddx3x*	Literature	TGGAAATAGTCGCTGGTGTG	GGAGGACAGTTGTTGCCTGT	Lennox *et al.* (PubMed ID:32135084)
Up	*Donson*	Commercial			OriGene;MP203922
Up	*Slc38a5*	Commercial			OriGene;MP215857
Up	*Alad*	Commercial			OriGene;MP200605
Down	*Fam117a*	Commercial			OriGene;MP214105
Down	*Ell2*	Literature	CGCTGGAGACTTACCAGAGC	CATTGAAGGGATCATTTTTGG	Pascal *et al.* (PubMed ID:28870994)
Down	*Dnmt1*	Literature	CCCATGCATAGGTTCACTTCCTTC	TGGCTTCGTCGTAACTCTCTACCT	Noh *et al.* (PubMed ID:15671176)
Down	*Ube2o*	Commercial			OriGene;MP217952

Supplemental Table 2

qPCR Primers for β-like globin profiling

Description	Gene	Forward primer seq	Reverse primer seq
Mus musculus *β* globin	*εy*	TGGCCTGTGGAGTAAGGTCAA	GAAGCAGAGGACAAGTTCCCA
	βh1	TGGACAACCTCAAGGAGACC	ACCTCTGGGGTGAATTCCTT
	βmajor/minor	TTTAACGATGGCCTGAATCACTT	CAGCACAATCACGATCATATTGC
Homo sapiens *β* globin	*ε (HBE)*	GCAAGAAGGTGCTGACTTCC	ACCATCACGTTACCCAGGAG
	y (HBG)	TGGATGATCTCAAGGGCAC	TCAGTGGTATCTGGAGGACA
	β (HBB)	CTGAGGAGAAGTCTGCCGTTA	AGCATCAGGAGTGGACAGAT

Supplemental Table 3

Guide RNA (gRNA) Sequences for CRISPR/Cas9 Knockout (KO)

Name	sgRNA sequence
gAAVS1	GGACGCACCATTCTCACAAA
gDIS3L2 No.1	TTCCCCAGAGCATAGCAGCG
gDIS3L2 No.2	AATACTAACAGAGTATGGCG
gZCCHC6 No.1	TTGACTGTTGATCAGAAACG
gZCCHC6 No.2	TGAGTCTGTACTTTCAACGA